DEFENCE **R&D** DÉFENSE

Military Voice Services over Wireless ATM Networks: ATM Adaptation Layer Study

Luis Villasenor-Gonzalez and Louise Lamont
Communications Research Centre Canada

CRC Communications
Research Centre
Centre de recherches
sur les communications

Defence R&D Canada
DEFENCE RESEARCH ESTABLISHMENT OTTAWA

National Défense
Defence nationale

Canadä

20011105 012

DEFENCE <img> DÉFENSE

Military Voice Services over Wireless ATM Networks: ATM Adaptation Layer Study

Luis Villasenor-Gonzalez and Louise Lamont
Broadband Network Technologies
Communications Research Centre Canada

CRC Communications
Research Centre
Centre de recherches
sur les communications

DEFENCE RESEARCH ESTABLISHMENT OTTAWA

Abstract

ATM technology has enjoyed great success, due in great part, for its ability to support a whole range of applications with Quality of Service (QoS) guarantees. Consequently, ATM has become of great interest for the support of services over military telecommunications networks.

This report is provided as part of a study on the feasibility of military voice services over wireless ATM networks. In this study we are concerned with the support of low data rate and delay sensitive applications over wireless ATM link, where the ATM Adaptation Layer 2 has been identified as a suitable adaptation layer for the support of such type of traffic. Nevertheless, as currently specified, AAL2 does not provide any protection mechanisms to allow for its efficient implementation over the wireless medium. The work presented in this document includes performance analysis results to evaluate the implementation of *Forward Error Correction* (FEC) codes, diversity reception mechanisms and/or protocol enhancements to improve the performance of AAL2 over a wireless ATM network.

Résumé

Le mode de transfert asynchrone (MTA) a connu beaucoup de succès, en grande partie parce qu'il convient à toute une gamme d'applications comportant des garanties de qualité de service. Il est donc d'un grand intérêt pour la prestation de services sur les réseaux de télécommunications militaires.

Le présent rapport fait partie d'une étude de la faisabilité de services vocales à usage militaire empruntant des réseaux MTA sans fil. L'étude porte plus précisément sur le fonctionnement d'applications sensibles aux retards et à faible débit binaire empruntant une liaison MTA sans fil, dans un contexte où la couche d'adaptation MTA 2 (CAM2) serait la couche d'adaptation utilisée pour la prise en charge de ce genre de trafic. Selon ses caractéristiques actuelles, la CAM2 ne comporte pas les mécanismes de protection nécessaires pour permettre une mise en œuvre efficace dans un milieu sans fil. Il est fait état des résultats d'une analyse de la qualité de transmission effectuée pour évaluer la possibilité d'utilisation de codes de *correction d'erreurs sans voie de retour* (aussi dite correction d'erreur directe ou CED), de techniques de réception en diversité ou de modifications du protocole pour améliorer la qualité de transmission assurée par la CAM2 sur un réseau MTA sans fil.

Executive Summary

Wireless and personal communication systems, such as Wireless LANs (WLANs), are experiencing enormous growth due to their particular characteristics, such as lower implementations costs, higher flexibility and the capability to support and manage mobile users. In this scenario, the use of Wireless ATM (WATM) can be viewed as an efficient way for wireless users to access an ATM network. WATM standardization is currently being studied by the WATM Working Group under the auspices of International Telecommunications Union (ITU-T). Systems are being analyzed in which the radio channel allows a mobile user to access the ATM network, but the use of a wireless link can be useful also when mobility is not required. Wireless solutions can also prove advantageous in other cases, for example when the installation of wired links is too expensive, technically difficult or prohibited by architectural constraints. In these cases a wireless link with fixed transmitter and receiver placed between two nodes of the ATM network can represent an interesting and economical solution.

This document discusses the concepts related to the ATM Adaptation Layer (AAL) and, in particular, details the use of the ATM Adaptation Layer 1 (AAL1) and the ATM Adaptation Layer 2 (AAL2) to adapt voice for ATM networks. ATM networks carry fixed size cells within the network regardless of the application in use. The use of ATM Adaptation Layers AAL-1, AAL-3/4 and AAL-5 for voice services may allow for a partial fill of ATM cells resulting in inefficient use of the bandwidth. When many connections share a common path between ATM end-points, it is possible to avoid this inefficiency by multiplexing the connections into a single ATM connection. This approach can be quite useful when the ATM network comprises of wireless links of limited bandwidth. The ATM Adaptation Layer 2 (AAL2) provides multiplexing capabilities by assembling variable size packets from different users into an ATM cell payload and transmitting the cells on the same ATM Virtual Channel Connection (VCC). Nevertheless, as currently specified, AAL2 does not provide any protection mechanisms to allow for its efficient implementation over the wireless medium. If the ATM cells are to be filled with information belonging to different users, and then transmitted over a wireless link, a number of important aspects must be considered, such as, the amount of error protection, the method of packet delineation and the QoS management of each call. These choices determine the overall efficiency of the system.

The work presented in this document includes the analytical characterization of the wireless channel. This characterization is used in the derivation of numerical results, which are presented to demonstrate the performance of the AAL2. For the analysis, several performance metrics are presented to evaluate the probability of lost AAL2 packets and the probability of errors over the payload of AAL2 packets. In addition, different scenarios are presented to evaluate the use of forward error correction (FEC) codes, diversity reception mechanisms and protocol enhancements to improve the performance of AAL2 over the wireless medium.

Sommaire

Les systèmes de communications personnelles et les systèmes sans fil, tels les réseaux locaux sans fil (WLAN), connaissent une croissance énorme en raison de leurs caractéristiques, notamment coût de mise en place inférieur, adaptabilité supérieure et capacité de prise en charge et de gestion d'utilisateurs itinérants. Dans ce contexte, l'utilisation du MTA sans fil peut donc sembler un moyen efficace de permettre à des utilisateurs du sans-fil d'avoir accès à un réseau MTA. Le Groupe de travail sur le MTA sans fil se penche à l'heure actuelle sur la normalisation de cette technique, sous les auspices de l'Union internationale des télécommunications (UIT-T). On analyse des systèmes où le canal radio permet à l'utilisateur mobile d'avoir accès au réseau MTA. Toutefois, l'emploi d'une liaison sans fil peut être utile même quand il n'est pas nécessaire d'être mobile. Il peut aussi s'avérer avantageux dans d'autres cas, notamment lorsque l'installation de liaisons filaires est trop coûteuse ou difficile à réaliser d'un point de vue technique ou encore que des contraintes architecturales la rende impossible. En pareil cas, une liaison sans fil avec émetteur et récepteur fixes entre deux nœuds du réseau MTA peut offrir une solution économique intéressante.

Le présent rapport aborde les concepts liés à la couche d'adaptation MTA (CAM) et s'attarde, en particulier, sur l'utilisation de la couche d'adaptation MTA 1 (CAM1) et de la couche d'adaptation MTA 2 (CAM2) pour adapter la communication vocale aux réseaux MTA. Le réseau MTA achemine des cellules de taille fixe indépendamment de l'application en usage. L'utilisation des CAM1, CAM3/4 et CAM5 pour les services de la voix ne permet pas toujours de remplir les cellules MTA, ce qui mène à un usage inefficace de la bande assignée. Quand plusieurs connexions partagent un même trajet entre deux extrémités MTA, il est possible d'éviter cette inefficacité en fondant les connexions en une connexion MTA unique par multiplexage. Cette méthode peut être très utile lorsque le réseau MTA se compose de liaisons sans fil à bande de largeur limitée. La CAM2 permet le multiplexage grâce à l'assemblage des paquets de tailles diverses de différents utilisateurs en une cellule MTA renfermant les données utiles, les cellules constituées étant ensuite transmises par la même connexion de canal virtuel. Toutefois, selon ses caractéristiques actuelles, la CAM2 ne comporte pas les mécanismes de protection nécessaires pour permettre une mise en œuvre efficace dans un milieu sans fil. Pour remplir les cellules MTA des données appartenant à différents utilisateurs et les transmettre ensuite au moyen d'une liaison sans fil, il faut tenir compte d'un certain nombre de considérations importantes, telles la protection contre les erreurs, la méthode de délimitation des paquets et la gestion de la qualité de service de chaque appel. Les choix effectués à ces égards déterminent l'efficacité d'ensemble du système.

Les travaux dont il est fait rapport ici comprennent une vérification analytique des caractéristiques du canal sans fil. Cette caractérisation permet d'arriver à des valeurs numériques qui servent à démontrer la qualité de transmission assurée par la CAM2. Pour les besoins de l'analyse, les auteurs se reportent à plusieurs mesures de la qualité afin d'évaluer la probabilité de pertes de paquets CAM2 et la probabilité d'erreurs de transmission des données utiles que renferment ces paquets. Ils présentent également différents scénarios afin d'évaluer l'utilisation de codes de correction d'erreurs sans voie de retour (aussi dite correction d'erreur directe ou CED), de techniques de réception en diversité et de modifications du protocole pour améliorer la qualité de transmission assurée par la CAM2 dans un milieu sans fil.

Acknowledgments

Remerciements

TABLE OF CONTENTS

List of Figures

List of Tables

1 INTRODUCTION

The Asynchronous Transfer Mode (ATM) technology is widely used over public and private telecommunication systems all over the world. One of the main reasons for the great success of ATM is because of its ability to support a whole range of applications with Quality of Service (QoS) guarantees. Throughout the years there has been a great deal of investment in terms of research, equipment development and deployment, and recently there has been great interest in the use of ATM over military telecommunication networks. Several authors have proposed the use of ATM over strategic and tactical military networks arguing that implementing a well-known and tested technology would greatly reduce costs. Additionally the use of ATM can increase the interoperability between strategic and tactical nodes, as well as, the interconnectivity with civilian telecommunication networks.

Due to the nature of military telecommunication networks, tactical networks require the support for communication between mobile nodes. Usually, these mobile nodes require the use of wireless telecommunications links, which are limited in bandwidth and present a much higher *bit error rate* (BER) than that of wired links. On the other hand, ATM was initially conceived to be used over high reliable links, such as fiber-optic links, with BER in the order of 10^{-10} or less. If ATM is to be used over wireless links, then several technical issues must first be resolved for the successful deployment of ATM over strategic and tactical networks. The use of ATM Adaptation Layers AAL-1, AAL-3/4 and AAL-5 for voice services may allow for a partial fill of ATM cells resulting in inefficient use of the bandwidth. When many connections share a common path between ATM end-points, it is possible to avoid this inefficiency by multiplexing the connections into one ATM connection. This approach can be quite useful when the ATM network comprises of wireless links of limited bandwidth. The ATM Adaptation Layer 2 (AAL2) provides multiplexing capabilities by assembling variable size packets from different users into an ATM cell payload and transmitting the cells on the same ATM Virtual Channel Connection (VCC). If the ATM cells are to be filled with information belonging to different users, and then transmitted over a wireless link, a number of important aspects must be considered, such as, the amount of error protection, the method of packet delineation and the QoS management of each call. These choices determine the overall efficiency of the system.

This reports begins with a discussion of different mechanisms used for the transmission of voice traffic over ATM networks. Section 2 presents a brief description of some schemes used for the transport of voice traffic. Section 3 and 4 provide a detailed description of the ATM Adaptation Layers 1 and 2 standards, as well as, an overview of some network topologies (scenarios) of interest. In Section 5, several issues of concern with respect to the use of AAL2 over wireless ATM (WATM) are presented. Section 6 describes the analytical characterization of a wireless channel and Section 7 presents the performance analysis of AAL2 over WATM. Finally, Section 8 presents recommendations for the implementation of AAL2 over wireless ATM networks.

2 BACKGROUND

Currently, two standards are used for the efficient transport of voice traffic over ATM networks; namely the AAL1 and the AAL2 standards [1][2]. A brief description of these standards is provided in this section followed by detail descriptions in Sections 3 and 4.

The ATM Adaptation Layer 1 is well suited to transport voice over ATM networks. This is done using AAL1 Circuit Emulation or AAL1 Structured Circuit Emulation. Circuit Emulation allows the user to establish an AAL1 ATM connection to support a circuit, such as a full T1 or E1, over the ATM backbone. On the other hand, Structured Circuit Emulation establishes an AAL1 N x 64 kb/s circuit, such as fractional T1 or E1, over the ATM backbone.

2.1 AAL1: Circuit Emulation

Circuit emulation maps an entire T1 or E1 circuit to a single ATM Virtual Circuit (VC). An AAL1 Constant Bit Rate (CBR) connection can be used to support circuit emulation. This type of connection is typically used to carry end-to-end transparent circuits between Time Division Multiplexers (TDMs) or digital Public Branch Exchanges (PBXs) over an ATM backbone. Circuit Emulating is an easy way to interface to an ATM backbone; but is inefficient because it uses more bandwidth than the bandwidth required transporting voice over a Public Switched Telephone Network (PSTN) due to ATM overhead. The overhead incurred when encapsulating voice into ATM's 53-byte cell requires 13% more bandwidth than the circuit it is carrying because of the 5 byte ATM header and 1 byte AAL1 header that is added to each 47-byte payload. In addition, the bandwidth is permanently allocated even if there are no active voice calls. Furthermore, bandwidth allocation cannot be modified to meet the applications changing requirements. On the other-hand, circuit emulation introduces minimal delay as the T1 or E1 bit stream is processed and segmented without regard to the framing structure in the circuit. Figure 1 shows a basic Circuit Emulation application example [5].
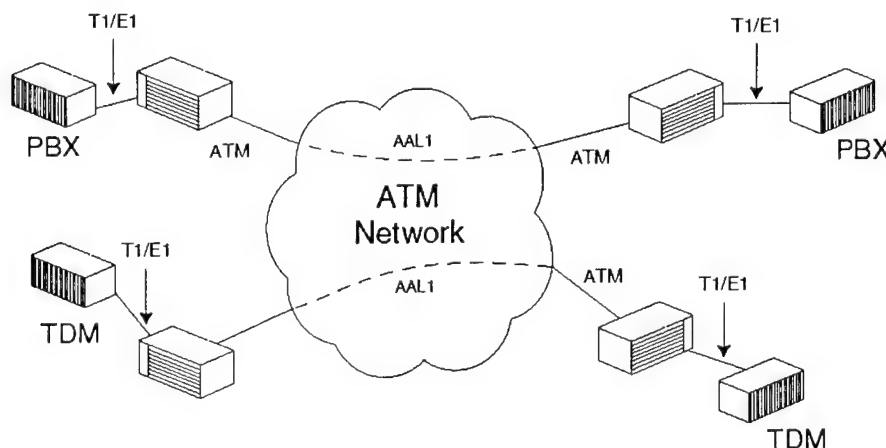
Figure 1: Circuit emulation application.

2.2 AAL1: Structured Circuit Emulation

Structured circuit emulation maps individual 64 kb/s circuits in a T1 or E1 line to ATM VCs. Thus, individual groups of timeslots are mapped to properly sized ATM circuits, thus allowing for an improved utilization of bandwidth as compared to circuit emulation mode.

Structured circuit emulation provides improved granularity for establishing fractional T1 or E1 circuits over ATM networks. The drawback is that each timeslot must be recognised to allow routing of individual channels between PBX trunks. This means that one ATM cell can carry information from only one channel, as AAL1 does not provide any mechanism to identify multiple channels (users) within the payload of the ATM cell. On the other hand, if an ATM cell is to be completely filled with information from a single channel before being sent, one must wait 47 sample times before it is completely filled. Each timeslot contains a 1-byte sample and an ATM cell holds 47 bytes of payload information (plus 5 bytes of ATM header and 1 byte of AAL1 header). The end-to-end delay is therefore increased compared with the circuit emulation mode. To reduce the end-to-end delay partially filled ATM cells may be transmitted, however this approach results in an inefficient use of the bandwidth. Figure 2 shows a basic Structured Circuit Emulation application example [5].
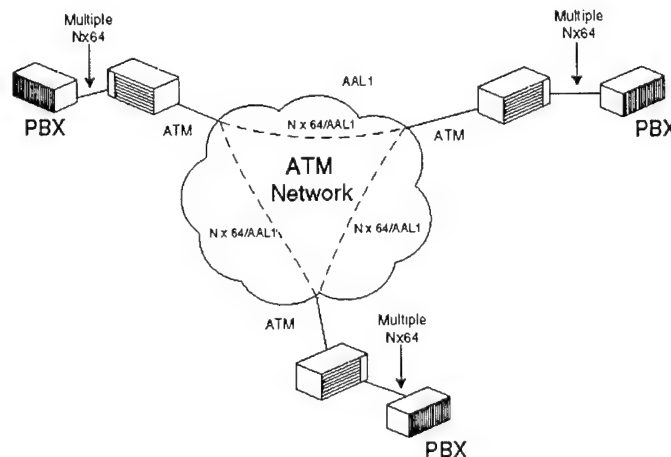
Figure 2: Structured Circuit Emulation application.

Overall, AAL1 Circuit Emulation is the most efficient way to transport full T1 or E1 circuits over an ATM backbone between two points in terms of reduced overhead and packetization delay.

2.3 AAL2

AAL2 was defined to provide for an efficient transport of low data rate and delay sensitive traffic, including voice services, over ATM networks. AAL2 provides bandwidth-efficient transmission of variable size packets by multiplexing the delay sensitive traffic from different users on a single ATM connection. AAL2 is not limited to ATM connections using the CBR traffic class but it also supports Variable Bit Rate (VBR) ATM traffic class. Under AAL2, bandwidth utilization is improved by the support of silence suppression and voice compression techniques.

3 ATM ADAPTATION LAYER 1

The ATM Adaptation Layer 1 (AAL1) is defined in ITU-T Recommendation I.363.1 [1], and provides for the following services to the AAL user:

- Transfer of Service Data Units (SDU) with a constant source bit rate and their delivery with the same bit rate.
- Transfer of timing information between source and destination.
- Transfer of structure information between source and destination.
- Indication of lost or erred information not recovered by AAL1.

Section 3.1 provides a detail overview of the frame structure of AAL1, as standardised in ITU-T recommendation I.363.1. In addition, Section 3.2 presents several scenarios of interest for the implementation of AAL1 over ATM networks.

3.1 ITU-T Recommendation I.363.1 (AAL1)

The information payload contained within each ATM cell is set by the basic structure of AAL1 shown in Figure 3.

SN - Sequence Number
SNP - Sequence Number Protection
SAR-PDU - Segmentation And Reassembly Protocol Data Unit
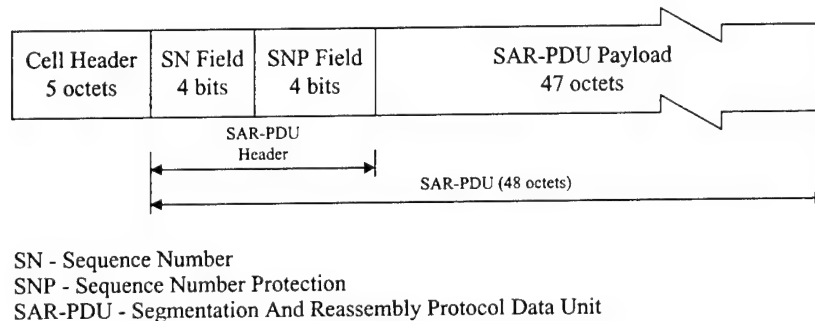
Figure 3: AAL1 SAR-PDU.

The information payload for AAL1 is 47 octets. Optional structures for AAL1 add additional overhead, reduce the information payload, and are used for structured circuit emulation. The Sequence Number (SN) field is used as a count value by the Convergence Sublayer (CS) to detect lost or misinserted SAR-PDU payloads. The Sequence Number Protection (SNP) provides error detection and correction capabilities over the SAR-PDU header.

When assessing the use of AAL1 for Voice-Over-ATM, it is important to note that the AAL1 protocol has the following limitations:

- Only a single user of the AAL can be supported.
- Reducing delay requires significant additional bandwidth, as ATM cells must be sent before filling the AAL1 payload field.
- Bandwidth is used even when there is no traffic.

4

- Voice is always 64 kb/s or bundles of 64 kb/s (N x 64).
- There is no standard mechanism in the AAL1 structure for compression, idle channel removal, silence detection/suppression or Common Channel Signalling (CCS).

3.2 AAL1 Scenarios

Some applications are adequately supported by AAL1. A typical application is one that interconnects a Public Voice Switch to an Internet Service Provider (ISP) using an ATM backbone network as shown in Figure 4 [5]. In this application, the traffic over the ATM network is entirely modem data, which is adequately served with AAL1, as modem data cannot take advantage of the statistical gain achieved by silent suppression techniques associated with voice traffic.
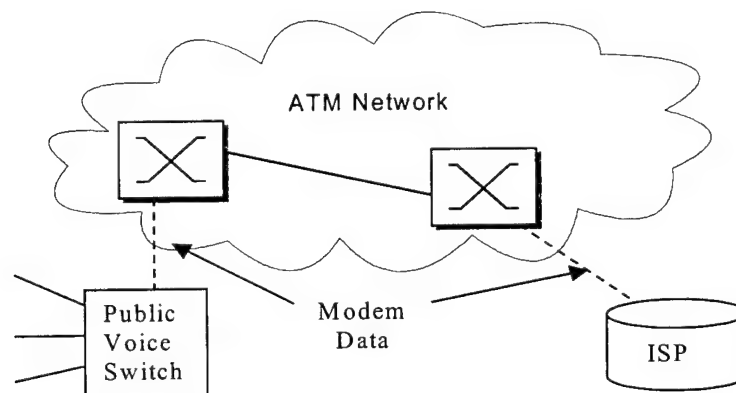
Figure 4: Internet Access via an ATM Backbone.

The use of AAL1 is also well suited for applications in which the ATM network provides the functionality of a Digital Cross-Connect System in TDM networks, as shown in Figure 5 [5]. In this scenario ATM cells, carrying information from individual T1 or E1 channels, can be switched to any port of the ATM Cross-Connect system. In this scenario the ATM network allows for the interconnection of PBXs, Time Division Multiplexers (TDMs), channel banks and other traditional voice/data equipment, by providing routing for DS0s or N x DS0s.
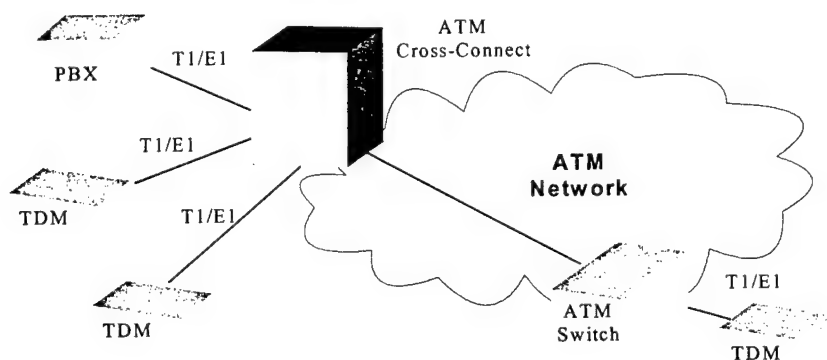
Figure 5: ATM cross-connect topology.

5

4 ATM ADAPTATION LAYER 2

The ATM Adaptation Layer 2 (AAL2) has been standardised, under recommendation I.363.2, by the ITU-T for the support of low data rate and delay sensitive traffic over ATM Networks. AAL2 can provide significant improvement in bandwidth utilization that is not attainable by using other previously defined ATM Adaptation Layer, such as, AAL1, AAL3/4 or AAL5.

Section 4.1 provides a detailed overview of the frame structure of AAL2, as standardised in ITU-T recommendation I.363.2. In addition, Section 4.2 presents several scenarios of interest for the implementation of AAL2 over ATM networks.

4.1 ITU-T Recommendation I.363.2 (AAL2)

AAL2 is divided into two sublayers: the Common Part Sublayer (CPS) and the Service Specific Convergence Sublayer (SSCS) as shown in Figure 6 [2].

Different SSCS protocols may be defined to support specific AAL2 user services, or groups of services. The SSCS may also be null, merely providing for the mapping of the equivalent AAL primitives to the AAL2 CPS primitives and vice versa. A null SSCS is used in most mobile voice applications [6].

CPS Common Part Sublayer
SAP Service Access Point
SSCS Service Specific Convergence Sublayer
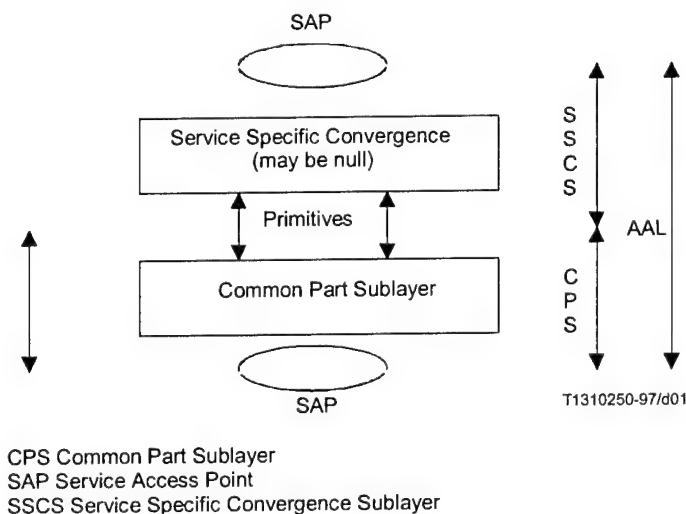
Figure 6: Structure of the AAL2.

The AAL2 users have the capability to select a given AAL Service Access Point (SAP) associated with the QoS required to transport the Service Data Units (SDUs) (see Figure 7). The AAL2 makes use of the service provided by the underlying ATM layer. Multiple AAL connections may be multiplexed into a single ATM layer connection at the Common Part Sublayer (CPS) of AAL2.

6
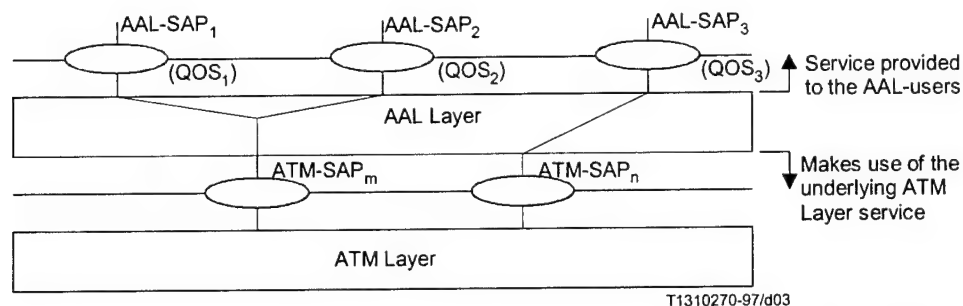
NOTE – How QoS at the AAL-SAP is mapped into the ATM-SAP QoS in the event of multiplexing in the AAL is for further study.

Figure 7: Relation between AAL-SAP and ATM-SAP.

The CPS layer enables variable size packets (0-64 bytes) from different users to be assembled in an ATM cell payload and transmitted on the same VCC.

The CPS provides the functionality for:

- Identifying the users of the AAL,
- Assembling/disassembling the variable payload associated with each user,
- Error detection,
- A link between the CPS and the appropriate SSCS.

A CPS packet, associated with a single AAL2 user, consists of a 3-octet CPS-Packet Header (CPS-PH) followed by a CPS-Packet Payload (CPS-PP). Key fields of the CPS packet are the Channel Identifier (CID), the Length Indicator (LI), the User-to-User Indication (UUI), and the HEC fields, as shown in Figure 8.

CID Channel Identifier (8 bits)
LI Length Indicator (6 bits)
UUI User-to-User Indication (5 bits)
HEC Header Error Control (5 bits)
CPS-INFO Information (1 .. 45/64 octets)
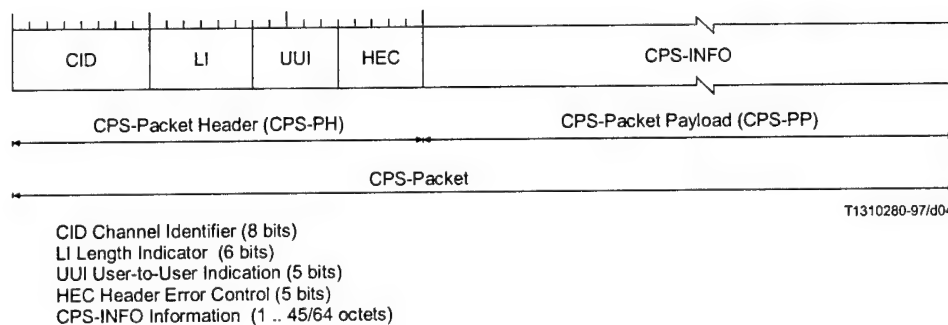
Figure 8: Format of AAL2 CPS-Packet.

7

The CID Field uniquely identifies the individual user channels within the AAL2. The LI Field identifies the length of the packet payload associated with each individual user. The value of the LI is one less than the packet payload. The UUI Field provides a link between the CPS and an appropriate SSCS that satisfies the higher layer application.

Following assembly, CPS packets are combined into a CPS-PDU payload, as shown in Figure 9. The CPS-PDU consists of a one-octet start field (STF) and a 47-octet payload. The 48-octet CPS-PDU is the ATM-SDU.

OSF Offset Field (6 bits)
SN Sequence Number (1 bit)
P Parity (1 bit)
PAD Padding (0 to 47 octets)
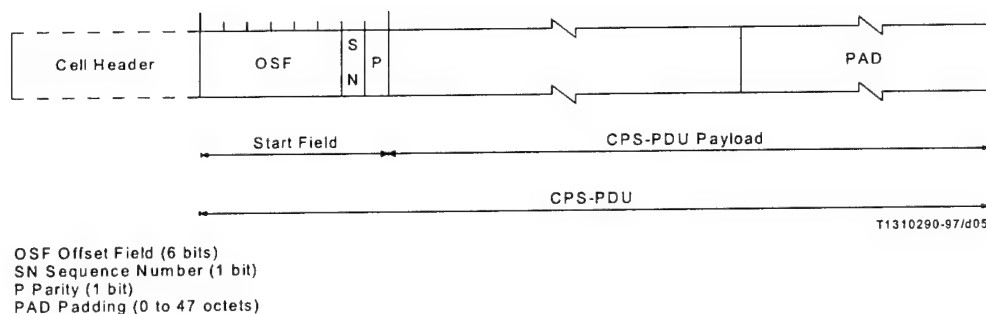
Figure 9: Format of CPS-PDU.

The Offset Field (OSF) identifies the beginning of a CPS packet within the CPS-PDU. The Sequence Number (SN) protects data integrity. The start field is protected against errors by the Parity bit.

4.2 AAL2 Scenarios

The Telecom and Wireless communities are investigating the use of AAL2. They have identified network scenarios where the use of AAL2 is anticipated. Such scenarios are the Private and Public Network Trunking and the International Mobile Telecommunications for the year 2000 (IMT-2000) network access.

4.2.1 Telecom Scenarios

The Telecom community foresees a number of scenarios where AAL2 may be used. One application example connects a PBX to a PSTN through an ATM network, to provide access to the PSTN services, as shown in Figure 10 [3].

A typical application is achieved by multiplexing a large number of narrowband channels over a broadband facility. Since the current generation of PBXs does not support ATM or AAL2, devices known as Interworking Function (IWF) perform interconnection to the ATM network. The broadband facility between IWFs may be any that provides ATM functionality, such as a direct physical connection, a Synchronous Optical Network (SONET) ring, or a full ATM network. The networks at the narrowband side may be PBXs or public or private networks of switches and may

8

connect to an IWF via one or more physical interfaces. These physical interfaces may be based on ISDN Common Channel Signalling (CCS) or may utilise Channel Associated Signalling (CAS). The ATM network may be a full network, a single ATM switching element, or simply a direct interconnection between a pair of IWFs.

Note: The narrowband signaling at both ends and the IWF-IWF signaling must be identical.
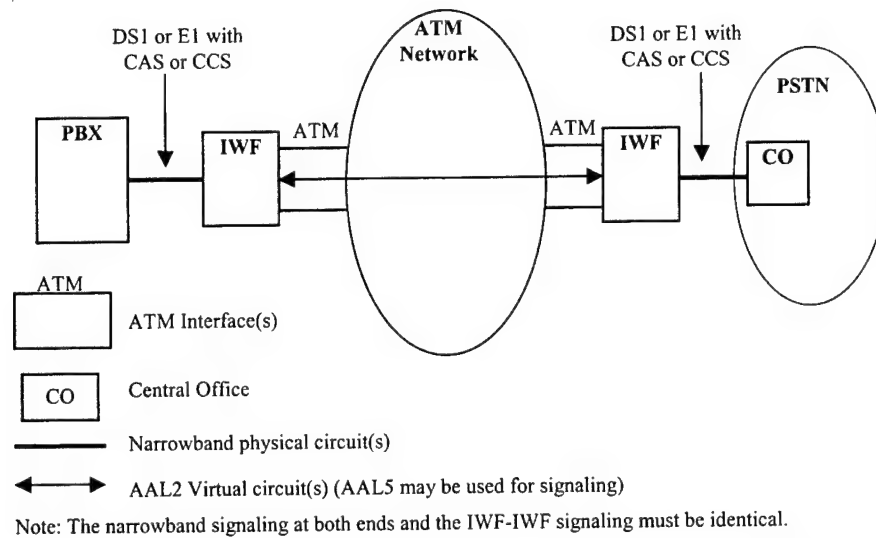
Figure 10: Access to the Public Switched Telephone Network (PSTN) by a PBX.

Another application example, shown in Figure 11, uses multiple IWFs to provide switched trunking between PBXs [3]. A group of IWFs are interconnected by an ATM network to form a network of IWFs. PBX connectivity is achieved by establishing one or more ATM VCCs using AAL2 between each pair of IWFs that need to communicate.
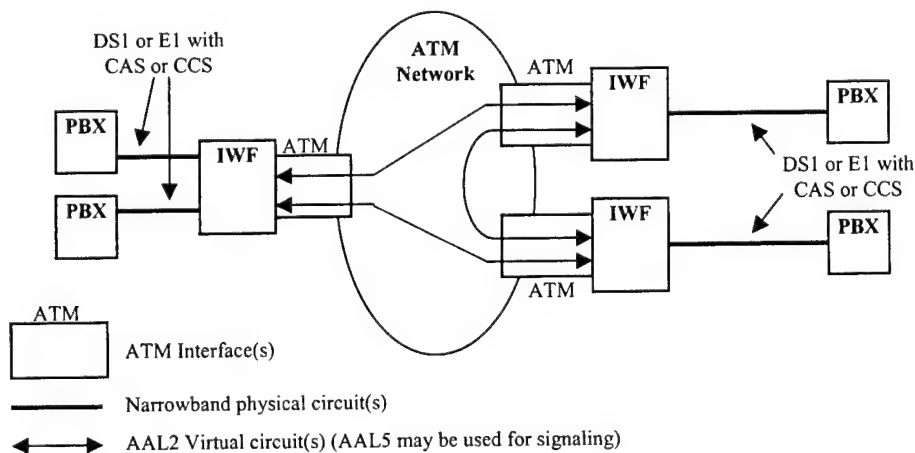
Figure 11: PBX-PBX Trunking.

9

The virtual circuits through the ATM network are Switched Virtual Connections (SVCs), Permanent Virtual Connections (PVCs), or Soft-Permanent Virtual Connections (SPVCs) carrying:

- bearer traffic and CAS using AAL2
- CCS using AAL2 or AAL5

When connecting PBXs, the basic unit in the transport system is the time-slot. Each time-slot corresponds to a 64 kb/s channel supporting a single conversation. The signalling protocol between the PBXs deals with the allocation and deallocation of time slots. In the AAL2 framework, the IWF maps a time-slot into an AAL2 channel.

4.2.2 Wireless Scenarios

In the Universal Mobile Telecommunications Systems (UMTS)/International Mobile Telecommunications for the year 2000 (IMT-2000) there is a need for handling switched AAL2 connections, between AAL2 end systems, over a network of AAL2 switches. An AAL2 end system can be a Base Station (BS), Radio Network Controllers (RNC), or a Mobile Switching Centre (MSC).

Figure 12 shows an example of how the wireless community intends to use AAL2 switching [7]. An ATM-based Radio Access Network (RAN) includes AAL2 switching systems such as RNCs, MSCs and standard ATM switching systems connected by ATM links. RNCs and MSCs are in the AAL2 network cloud and can function as AAL2 end systems. Base Stations (BSs) can also be part of the AAL2 network, but need not be. This hierarchy hides the RNC-BS interface from the network and enables any proprietary transport (AAL2, TCP/IP, etc) and addressing scheme to be used between a RNC and its BSs.
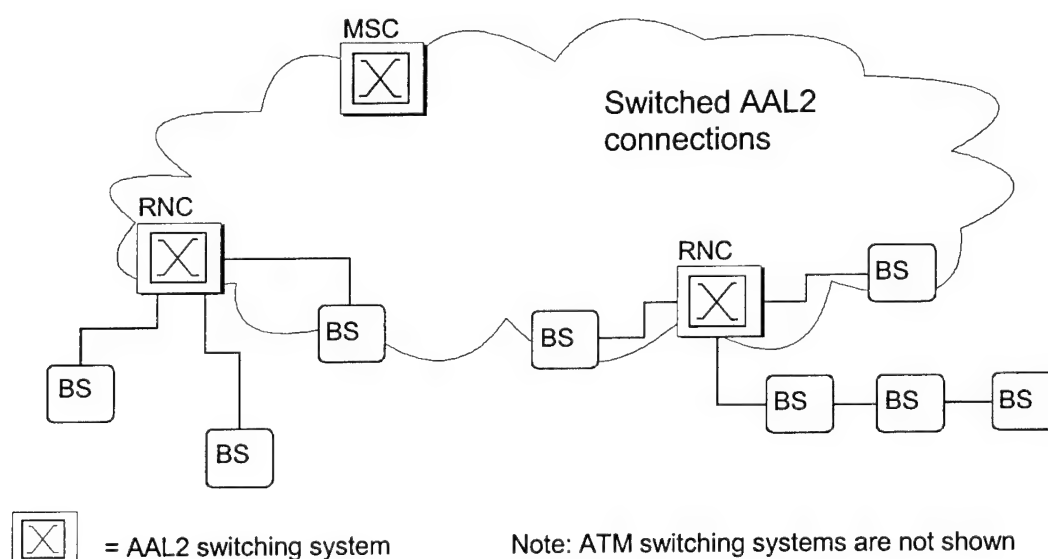
Figure 12: An ATM based Radio Access Network.

In the AAL2 network, packets are transferred between users by AAL2 switching, AAL2 trunking, or a combination of both. In AAL2 switching, packets encapsulated within an ATM cell are individually switched at the AAL2 nodes with the use of Virtual Path Identifier/Virtual Channel Identifier/Channel Identifier (VPI/VCI/CID) values. In AAL2 trunking, ATM cells containing the AAL2 information are switched at the ATM layer using the VPI/VCI values. AAL2 trunking ensures seamless connectivity. An end-to-end AAL2 connection is routed through a concatenation of Virtual Circuits (VCs) involving both ATM and AAL2 switching systems. The physical connections in the AAL2 network can be wireless or wired. Upon receiving an ATM cell, an AAL2 switching system performs AAL2 level switching, while an ATM switching system performs only ATM level switching.

In the UMTS/IMT2000 networks, the UNI is in the radio interface between the Mobile Terminal (MT) and the Base Station (BS). The AAL2 network does not include the radio interface; thus there is no interest of AAL2 signalling over UNI as it is shown in Figure 13 [4]. The MT may support for instance AAL1 or AAL5.
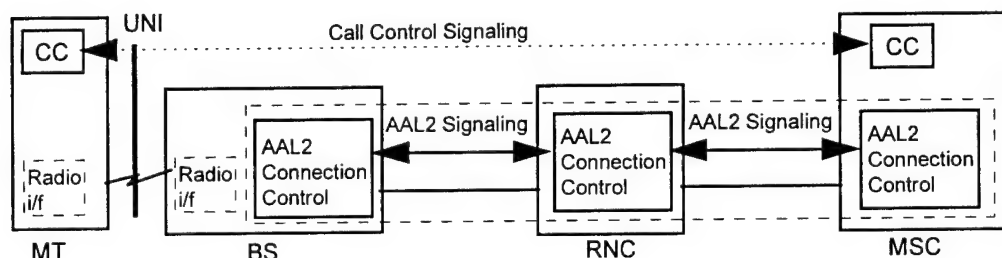
Figure 13: UNI in the radio interface between the Mobile Terminal and the Base Station.

5 AAL2 PERFORMANCE ISSUES

The multiplexing of information at the AAL provides advantages such as improved bandwidth utilisation. However a number of important aspects such as, the amount of error protection, the method of packet delineation and the guarantee of the QoS requirements of each call must be considered.

The architecture shown in Figure 14 has been used to identify several AAL2 issues of interest. In this architecture the wireless subsystems are interconnected to an ATM network through wireless ATM links. The wireless subsystems are basically cellular telephone systems where mobile communication stations (vehicles) are affiliated with a base station. The base station in a subsystem communicates with the Radio Access Point (RAP) using a 64 kb/s point-to-point link. The wireless connections between the RAP and the ATM backbone are typically Line of Sight (LOS) microwave links that operate between 64 kb/s and 2 Mb/s. Errors are bursty in nature and the BER varies from 10^{-3} to 10^{-6}. The base station in the wireless subsystem supports ATM and the RAP ATM switch supports AAL2.
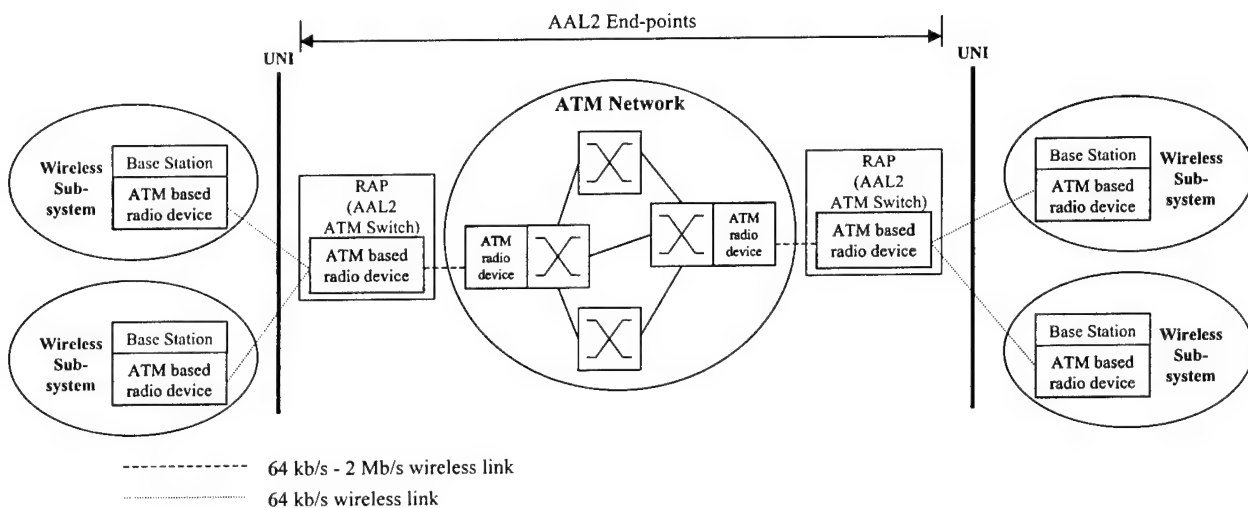
Figure 14: Tactical Architecture.

The following issues require careful evaluation to ensure that the AAL2 scheme works as well in a wireless environment as in a wired one and that the complexity of the scheme does not introduce any additional performance degradation.

1. The shared communication path must be long enough to justify the complexity of multiplexing and demultiplexing the traffic from different sources.

2. At the ATM layer, cell delineation must be addressed effectively in order to maintain acceptable delay characteristics. The cell delineation algorithm used in ATM is highly inefficient under high BER environments, as it is heavily dependant on recognising consecutive un-erred ATM cell headers to achieve synchronization.

3. Multiplexing of AAL2 connections may result in serious performance degradation when there are ATM cell losses. Currently, a single parity bit is used to detect errors in the STF field and a five-bit HEC code is used to detect errors in the AAL2 CPS packet header. These error detection schemes can be acceptable when the AAL2 connections are over fiber optic links, but when radio relay links are part of the AAL2 path a more robust error control mechanism is required to protect the headers within a cell.

4. The use of AAL2 introduces a delineation mechanism within the payload of each ATM cell. The delineation of AAL2 CPS Packets is vulnerable to bit errors, as AAL2 CPS packet headers do not provide any error correcting capability.

5. An AAL2 packet may sometimes be mapped across cell boundaries causing performance degradation, as payload padding may be required to fill the last ATM cell.

6. Providing QoS to individual users is a complex issue in AAL2. A single ATM cell carries packets from two or more users who may have different QoS requirements. Therefore the QoS requirements of the incoming streams must be considered when multiplexing is performed and an appropriate method for selecting the different streams is required.

7. The single bit sequence number in the AAL2 CPS-PDU header is insufficient to detect an even number of cell losses at the receiver. As a result partial information from two users will be assembled and sent to a single user.

8. AAL2 headers must be kept reasonable in size in order to provide a low overhead and at the same time be able to provide enough error protection to the users of the AAL.

In this report we only address those issues that are related to the performance of AAL2 in terms of CPS packet losses and CPS packet payload bit errors, as described in paragraph 3. In addition, we also address the performance degradation issues related to the delineation of AAL2 CPS packets, as described in paragraph 4.

13

6 WIRELESS CHANNEL CHARACTERIZATION

6.1 Introduction

Wireless links may be subject to a variety of transmission impairments such as fading, interference and noise. Some of these impairments exhibit a significant degree of correlation resulting in burst errors [8]. Analytical models based on Finite State Markov Chains (FSMC) have been widely used to characterize the *bit error process* of wireless communication channels.

Following the FSMC modeling approach, the wireless channel is characterized by a discrete-time Markov chain $\{C_n\}_{n\geq0}$, where C_n is a random variable associated with the state of the channel at time instant n. Random variable $\{C_n\}_{n\geq0}$ is defined in an N-dimensional state space $S = \{s_1, s_2, s_3, ..., s_N\}$, where $N \geq 2$. The time unit associated with transitions in the Markov chain can be defined to be equal to the transmission time of one bit, the transmission time of one packet, or any other time unit frame of interest. In the context of this work, the time unit associated with transitions of the Markov chain model is assumed to be equal to the transmission time of one bit, unless explicitly defined otherwise. In addition, each state s_k, $k = 1, 2, ..., N$ has an associated probability of bit error, which is directly related to the *bit error process* experienced at the receiving node.

The *bit error process* at the receiving node is defined by a discrete-time random variable $\{E_n\}_{n\geq0}$, where

$$E_n = \begin{cases} 0 & \text{If } n\text{ - th bit is not in error,} \\ 1 & \text{Otherwise.} \end{cases} \tag{1}$$

Figure 15 shows a simplified block diagram for the wireless channel, where X_n represents the information bits transmitted at time instants $n = 1, 2, 3, ...,$ over the wireless channel, and the received information bits are represented by $Y_n = X_n \oplus E_n$, where $\oplus$ is the *XOR* operator.

Wireless Channel

| Tx | $\{X_n\}_{n\geq1}$ → | FSMC state $\{C_n\}_{n\geq0} \rightarrow \{E_n\}_{n\geq0}$ | $\{Y_n = X_n \oplus E_n\}_{n\geq1}$ | Rx |
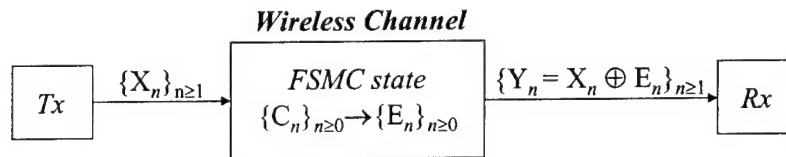
Figure 15: Wireless channel block diagram.

In this Section, two approaches are presented for the characterization of a wireless link using FSMC models. One of these approaches is based on modeling the *error-process* at the receiver by statistically characterizing the "birth" and "death" process of the *burst-error* and *error-free* events; the Gilbert-Elliott model [9, 10] is a common example of this approach. The second approach characterizes the *error-process* at the receiver by modeling the physical dynamics of the fading process. This last approach is considered a more general model for the characterization of the *error-process,* as the *burst-error* and *error-free* events are a function of the fading dynamics of the wireless link.

6.2 Gilbert-Elliott Model

The Gilbert-Elliott model is characterized by a two-state ($N = 2$) Markov chain $\{C_n\}_{n \geq 0}$, where C_n is a random variable associated with the state of the channel at time instant n, with state transition diagram as shown in Figure 16.
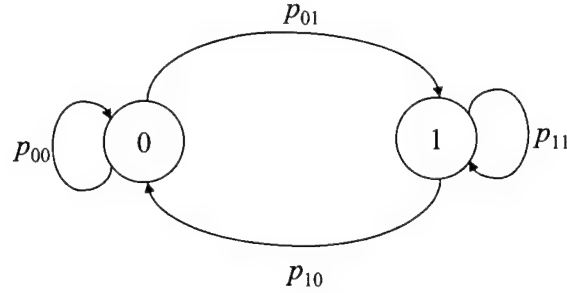
Figure 16: Gilbert-Elliott channel model.

Under the Gilbert-Elliott model, the physical channel assumes one of two states, one state is associated with a low probability of bit error (state 0 or *good* state), while the other state is associated to a high probability of bit error (state 1 or *bad* state), each heaving an associated error probability $P_e(k)$, $k = 0$, 1 and $P_e(0) \ll P_e(1)$. The transition probability matrix, **P**, of $\{C_n\}_{n \geq 0}$ is denoted by,

$$\mathbf{P} = \begin{bmatrix} p_{00} & p_{01} \\ p_{10} & p_{11} \end{bmatrix},$$ (2)

and the stationary probability vector π is given by,

$$\pi = \begin{bmatrix} \pi_0 & \pi_1 \end{bmatrix} = \begin{bmatrix} \dfrac{p_{10}}{p_{01} + p_{10}} & \dfrac{p_{01}}{p_{01} + p_{10}} \end{bmatrix}.$$ (3)

The steady state channel bit error rate (BER), ε, of the Gilbert-Elliott model is given by

$$\varepsilon = \frac{P_e(0) p_{10} + P_e(1) p_{01}}{p_{01} + p_{10}},$$ (4)

where $P_e(k)$ is the channel error probability in state k.

For Markov chain $\{C_n\}_{n \geq 0}$, the time spent in state 1 (0) is geometrically distributed with mean $1/p_{10}$ ($1/p_{01}$). The mean burst length, τ, for the model is considered to be the time spent in state 1, and is given by $\tau = 1/p_{10}$.

15

Under the Gilbert-Elliot channel model, the *bit error-process* $\{E_n\}_{n\geq0}$ at the receiver is a function of the channel state $\{C_n\}_{n\geq0}$ during which bit errors occur randomly with probability $P_e(k)$, $k = 0, 1$. Figure 17 shows a sample realization of the bit error process $\{E_n\}_{n\geq0}$. For a given channel bit error rate, ε, and selected values of $P_e(0)$ and $P_e(1)$ equations (2) and (3) are expressed in terms of the mean burst length, τ, by:

$$\mathbf{P} = \begin{bmatrix} 1-\alpha/\tau & \alpha/\tau \\ 1/\tau & 1-1/\tau \end{bmatrix},$$

(5)

$$\boldsymbol{\pi} = \begin{bmatrix} \dfrac{1}{1+\alpha} & \dfrac{\alpha}{1+\alpha} \end{bmatrix},$$

(6)

where α is defined as

$$\alpha = \frac{\varepsilon - P_e(0)}{P_e(1) - \varepsilon}.$$

(7)
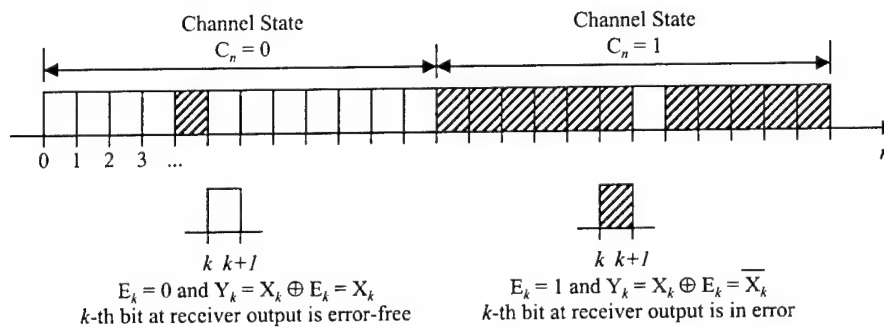
Figure 17: Sample realization of bit error process $\{E_n\}_{n\geq0}$.

6.3 Modeling the Fading Dynamics of the Channel

A Finite State Markov Chain (FSMC) model is derived from the fading dynamics of the channel by appropriately partitioning the dynamic range of the received Signal-to-Noise Ratio (*SNR*), γ, into a finite number, N, of non-overlapping intervals, such as, $[0, \gamma_1)$, $[\gamma_1, \gamma_2)$, ..., $[\gamma_{N-1}, \gamma_N)$, where $\gamma_N \to \infty$ [11]-[13], as shown in Figure 18. Each of the non-overlapping intervals represents a state in the resulting FSMC model and the channel is said to be in state $\{s_k\}$ if $\gamma \in [\gamma_{k-1}, \gamma_k)$.
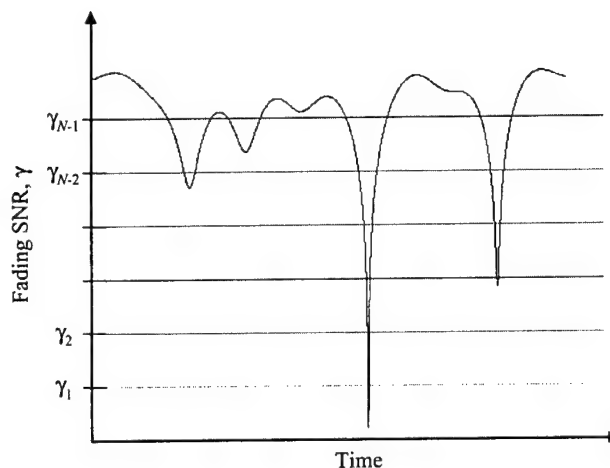
Figure 18: Partitioning of the fading dynamic range.

The FSMC model, characterizing the fading dynamics of the channel, is uniquely defined by its transition probability matrix **P**, the steady state vector π and the state error probability vector $\mathbf{P_e}$. The transition probability matrix, **P**, is defined as an $N \times N$ matrix with elements p_{ij}, $i,j = 1,2, ..., N$, where p_{ij} is defined as the probability of a transition from state i into state j, and is given by

$$p_{ij} = \frac{\Pr[\gamma_{i-1} \le \gamma_1 < \gamma_i, \gamma_{j-1} \le \gamma_2 < \gamma_j]}{\Pr[\gamma_{i-1} \le \gamma_1 < \gamma_i]} = \frac{\int_{\gamma_{j-1}}^{\gamma_j} \int_{\gamma_{i-1}}^{\gamma_i} p_{\Gamma_1, \Gamma_2}(\gamma_1, \gamma_2) d\gamma_1 d\gamma_2}{\int_{\gamma_{i-1}}^{\gamma_i} p_{\Gamma_1}(\gamma_1) d\gamma_1} , \qquad (8)$$

where $p_{\Gamma_1, \Gamma_2}(\gamma_1, \gamma_2)$ is the *joint probability density function* (jpdf) of Γ_1 and Γ_2, $p_{\Gamma_1}(\gamma_1)$ is the *probability density function* (pdf) of Γ_1 and Γ_1, Γ_2 are random variables defining the fading instants of interest.

According to [13] the partitioning of the fading dynamics of the channel can be done from the steady state probabilities of the FSMC, which can be evaluated following a recursive algorithm that is given by

17

$$\pi_k = \begin{cases} \dfrac{1}{2^N - 1} & k = 1 \\ 2 \cdot \pi_{k-1} & k = 1, 2, ..., N \end{cases} . \tag{9}$$

The state error probability vector, $\mathbf{P_e}$, is composed by elements $P_e(k)$, $k = 1, 2, ..., N$. It should be noted that the error probability $P_e(k)$, associated to each state $\{s_k\}$, is a function of the statistical time varying nature of the fading channel and is defined in terms of the *probability density function* characterizing the statistical fading dynamics of the channel. The error probability $P_e(k)$ is given by

$$P_e(k) = \frac{1}{\pi_k} \int_{\gamma_{k-1}}^{\gamma_k} p\text{r}(\gamma) \cdot e(\gamma) d\gamma, \tag{10}$$

where $p\text{r}(\gamma)$ is the *probability density function* (pdf) of the SNR, γ, and $e(\gamma)$ represents the error probability as a function of the SNR, γ, which is closely related to the *modulation/demodulation* scheme.

The probability of bit error, $e(\gamma)$, can be evaluated for many modulation schemes over *Additive White Gaussian Noise* (AWGN) and can be defined in terms of the Q-function, which is given by,

$$Q(x) = \int_x^\infty \frac{1}{\sqrt{2\pi}} \exp\left(-\frac{x^2}{2}\right) dx . \tag{11}$$

Table 1 shows the error probability, $e(\gamma)$, for some common modulation techniques.

Table 1: Bit error probability e(γ) for different modulation schemes.

Modulation Scheme	$e(\gamma)$
Binary Phase Shift Keying (BPSK)	$Q\left(\sqrt{2\gamma}\right)$
Quadrature Phase Shift Keying (QPSK)	$Q\left(\sqrt{2\gamma}\right)$
Coherent Binary Frequency Shift Keying (BFSK)	$Q\left(\sqrt{\gamma}\right)$
Non-coherent Binary FSK	$\dfrac{1}{2}\exp\left(\dfrac{\gamma}{2}\right)$

18

6.4 Modeling of Flat Fading Channels

6.4.1 Rayleigh Model

The *Rayleigh* distribution is commonly referred to model multipath fading with no direct line-of-sight (LOS) path by describing the statistical time varying nature of the fading amplitude, α, of a received signal over a flat fading channel. The *probability density function* (pdf) of a *Rayleigh* distributed random variable A, is given by [14, Eq. (2.6)]

$$p_A(\alpha) = \frac{2\alpha}{\Omega}\exp\left(-\frac{\alpha^2}{\Omega}\right), \quad \alpha \geq 0 \tag{12}$$

where $\Omega = \overline{\alpha^2}$ is the mean-square value of α.

Sometimes it is more convenient to work with the pdf of the SNR, γ, which is proportional to the square of the signal amplitude, α. The pdf a *Rayleigh* distributed random variable Γ, is given by [14, Eq. (2.7)]

$$p_\Gamma(\gamma) = \frac{1}{\overline{\gamma}}\exp\left(-\frac{\gamma}{\overline{\gamma}}\right), \quad \gamma \geq 0 \tag{13}$$

where $\overline{\gamma} = E[\gamma]$.

6.4.2 Nakagami-*n* (Rice) Model

When there is a dominant stationary (direct non-fading) signal component present, such as a line-of-sight (LOS) propagation path, the small scale fading amplitude distribution of the signal amplitude, α, follows a Nakagami-*n* (*Rice*) distribution. The *probability density function* (pdf) of a Nakagami-*n* distributed random variable, A, is given by [14, Eq. (2.15)]

$$p_A(\alpha) = \frac{2(1+n^2)e^{-n^2}\alpha}{\Omega}\exp\left[-\frac{(1+n^2)\alpha^2}{\Omega}\right]I_0\left(2n\alpha\sqrt{\frac{1+n^2}{\Omega}}\right), \quad \alpha \geq 0 \tag{14}$$

where $I_0(\cdot)$ is the zero-order modified Bessel function of the first kind, and n is the Nakagami-*n* fading parameter, which ranges from 0 to ∞. The Nakagami-*n* fading parameter n is related to the *Ricean K* factor by $K = n^2$ [14].

The pdf for the SNR of a Nakagami-n distributed random variable Γ, is given by [14, Eq. (2.16)]

$$p_\Gamma(\gamma) = \frac{(1+n^2)e^{-n^2}}{\overline{\gamma}}\exp\left[-\frac{(1+n^2)\gamma}{\overline{\gamma}}\right]I_0\left(2n\sqrt{\frac{(1+n^2)\gamma}{\overline{\gamma}}}\right). \quad \gamma \geq 0 \tag{15}$$

6.4.3 Nakagami-m Model

The Nakagami-m distribution arises as an approximate solution to the general problem of the distribution of the magnitude of the sum of random vectors [15], whereas the *Rayleigh* and *Ricean* distributions are the particular solutions to the above problem [16].

One interesting characteristic of the Nakagami-m distribution is that it includes the *Rayleigh* distribution, as a special case ($m = 1$), and it also approximates the *Ricean* and *Lognormal* distributions [11]. Thus, analytical derivations following the Nakagami-m distribution can easily be generalized to evaluate the *Rayleigh* and the *Ricean* fading channels. The *probability density function* (pdf) of a Nakagami-m distributed random variable, A, is given by [14, Eq. (2.20)]

$$p_A(\alpha) = \frac{2\alpha^{2m-1}}{\Gamma(m)}\left(\frac{m}{\Omega}\right)^m \exp\left[-\frac{m\alpha^2}{\Omega}\right], \quad \alpha \geq 0 \tag{16}$$

where m is the Nakagami-m fading parameter, which ranges from ½ to ∞.

The pdf for the SNR of a Nakagami-m distributed random variable Γ, is given by [14, Eq. (2.21)]

$$p_\Gamma(\gamma) = \frac{(1+n^2)e^{-n^2}}{\overline{\gamma}}\exp\left[-\frac{(1+n^2)\gamma}{\overline{\gamma}}\right]I_0\left(2n\sqrt{\frac{(1+n^2)\gamma}{\overline{\gamma}}}\right). \quad \gamma \geq 0 \tag{17}$$

The Nakagami-m fading distribution can approximate the Nakagami-n (*Rice*) distribution by appropriately mapping the fading parameter n to m. This mapping is given by [14, Eq. (2.26)]

$$m = \frac{(1+n^2)^2}{1+2n^2}. \quad n \geq 0 \tag{18}$$

7 AAL2 PERFORMANCE ANALYSIS

7.1 Performance Analysis over the Markovian Channel

The analysis of AAL2 over the Markovian channel presented in the sequel considers the generic AAL2 CPS-PDU structure shown in Figure 19. The CPS-PDU payload is filled with CPS packets as described in Section 4.1. When CPS packets are unavailable, padding is used instead. A CPS-PDU payload filled completely with CPS packets is shown in Figure 19. The maximum number of CPS packets that are accommodated in the CPS-PDU payload depends on the size of the CPS packets. Because AAL2 allows for a CPS packet to be mapped across CPS-PDU payload boundaries, the CPS-PDU payload includes M bits from the last CPS packet of the previous CPS-PDU payload following the STF. Correspondingly, it is possible that the last CPS packet might extend into the payload of the next CPS-PDU.
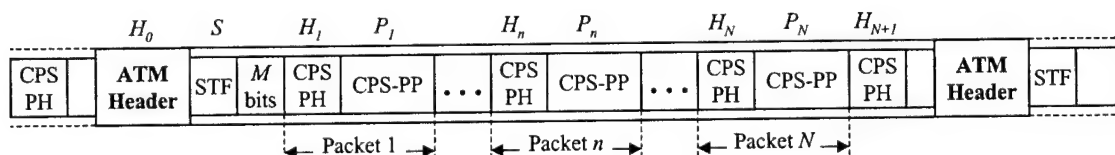
Figure 19: CPS PDU structure.

For convenience, the following notation is used to indicate the different fields in the ATM cell structure depicted in Figure 19:

- H_0 indicates the ATM cell header of size N_0 bits ($N_0 = 40$),
- S indicates the STF of size N_s bits ($N_s = 8$),
- H_n, $1 \leq n \leq N$, indicates the header of CPS packet n of size N_n bits ($N_n = 24$),
- P_n, $1 \leq n \leq N$, indicates the payload of CPS packet n of size L_n bits.

It is assumed that the payload of an AAL2 CPS packet is successfully delivered to the next higher layer when all the relevant header and control fields in the ATM cell and the CPS-PDU are correct. That is, successful delivery takes place when these fields are error-free or subject to correctable errors wherever error correction is applied (as may be the case, for example, with the ATM cell header). A CPS packet is considered lost (discarded) when at least one of the relevant header/control fields is subject to uncorrectable errors. For example, CPS packet payload P_1 is considered lost when any of H_0, S or H_1 is corrupted by errors. Similarly, CPS packet payload P_2 is lost when any of H_0, S, H_1 or H_2 is corrupted. In addition, undetectable errors are treated as a special case of uncorrectable errors. This observation is explained by the fact that the analysis relies on the bit error process over the channel (physical layer), which is characterized by the Markovian model. In this way, undetectable errors at the ATM or AAL2 layer are only the result of multiple bit errors (more than the error correcting capability of the header error control) over the channel and this case is accounted for as an uncorrectable error case.

21

The following random variable definitions are associated with CPS packets that lie completely in the payload of an ATM cell and are used in the analysis:

- β_n denotes a random variable that takes a value equal to zero (0) if CPS packet n is successfully delivered to the next higher layer and a value equal to one (1) otherwise. For example, $\beta_l = 0$ when payload P_l is delivered to the higher layers and $\beta_l = 1$ when payload P_l is discarded at the ATM or AAL layer.
- k_n denotes the number of errors in CPS packet payload P_n.

The joint probability distribution of (β_n, k_n) derived in the analysis presented below is used to obtain performance measures of interest at the AAL2. The analysis is based on the approach adopted in [17] for the performance evaluation of Wireless ATM at the ATM layer. In this work, the analysis presented in [17] is extended to address the effect of burst errors at the AAL2 layer.

The analysis is facilitated by defining $\phi_{ij}(k, n)$ as the probability that exactly k bits are in error in $\{0,1,..., n-1\}$ time-units and the channel state at time-unit n is j, $X_n = j$, given that channel state at time-unit 0 was i, $X_0 = i$ [17]. This quantity allows for keeping track of the state of the channel, as well as of the number of error occurrences in a block of n bits. $\Phi(k,n)$ is used to denote the matrix with elements $\phi_{ij}(k, n)$, $i, j = 1, 2, ..., N_c$, $n \geq 0$, $0 \leq k \leq n$, where N_c is equal to the number of states of the Markovian model. Matrix $\Phi(k,n)$ is computed by using the recursive algorithm presented in [18]. For $n = 0$, $k = 0$, $\Phi(0,0) = \mathbf{I}$, where $\mathbf{I}$ is the identity matrix. For $n > 0$,

$$\Phi(k,n) = \begin{cases} \Phi(k,n-1)\Delta_0 & k = 0 \\ \Phi(k,n-1)\Delta_0 + \Phi(k-1,n-1)\Delta_1, & 0 < k < n \\ \Phi(k-1,n-1)\Delta_1 & k = n \end{cases} \tag{19}$$

where Δ_0 and Δ_1 are defined as

$$\Delta_0 = (\mathbf{I} - \mathbf{P_e}) \cdot \mathbf{P}, \quad \Delta_1 = \mathbf{P_e} \cdot \mathbf{P}, \tag{20}$$

and

$$\mathbf{P_e} = diag\{P_e(1), P_e(2),..., P_e(N_c)\}. \tag{21}$$

Matrix Δ_0 accounts for the probability of no error occurrence during a one step transition, while matrix Δ_1 accounts for the probability of error occurrence during a one step transition.

The joint probability distribution of (β_n, k_n), $P[\beta_n, k_n]$, is easily evaluated as follows:

for $n = 1$

$$P[\beta_1 = 0, k_n = \ell] = \sum_{i_0=0}^{1} \pi \Phi(i_0, N_0)\Phi(0, N_S)\mathbf{P}^M \Phi(0, N_1)\Phi(\ell, L_1)\mathbf{e}, \tag{22}$$

22

for $1 < n \le N$

$$P[\beta_n = 0, k_n = \ell] = \sum_{i_0=0}^{1} \boldsymbol{\pi}\Phi(i_0, N_0)\Phi(0, N_S)\mathbf{P}^M \prod_{j=1}^{n-1} \Phi(0, N_j)\mathbf{P}^{L_j}\Phi(0, N_n)\Phi(\ell, L_n)\mathbf{e} \qquad (23)$$

,

$$P[\beta_n = 1, k_n = \ell] = \boldsymbol{\pi}\Phi(\ell, L_n)\mathbf{e} - P[\beta_n = 0, k_n = \ell]. \qquad (24)$$

where $\boldsymbol{\pi}$ is the steady state probability vector of $\{X_n, n \ge 0\}$, $\mathbf{P}^M$ is the M-step transition probability matrix and $\mathbf{e} = [1, 1, \ldots, 1]^T$ is the unit column vector of dimensions $N_c \times 1$.

The product $\Phi(i_0, N_0)\Phi(0, N_S)\mathbf{P}^M\Phi(0, N_1)\Phi(\ell, L_1)$ in Equation (22) is associated with the joint probability distribution of having i_0 errors in the ATM header, no errors in STF, no errors in the first CPS packet header and ℓ errors in the first CPS packet payload when there are M bits between the STF and the first CPS-PH. The single bit error correcting capability of standard ATM HEC encoding has been applied in the derivation of the expressions above as reflected by the choice of values for index i_0 in Equations (22) and (23). The STF as well as the CPS packet header, as defined in the ITU-T standard [2], do not provide for any error correction capability. It is assumed that a single bit error in the STF will disrupt the CPS packet delineation process causing the discarding of the entire CPS-PDU payload.

The joint probability distribution $P[\beta_n, k_n]$ for random channel errors is obtained from Equations (22)-(24) by replacing the occurrences of matrix $\Phi(k, n)$ by the scalar quantity $\Phi(k, n)$ representing the probability that there are k random errors in n bits:

$$\Phi(k, n) = \binom{n}{k}\varepsilon^k \cdot (1 - \varepsilon)^{(n-k)}, \qquad (25)$$

where ε is the channel BER. Thus, in the case of random errors Equations (22)-(24) become:

$$P[\beta_n = 0, k_n = \ell] = \sum_{i_0=0}^{1} \Phi(i_0, N_0)\Phi(0, N_S)\prod_{j=1}^{n} \Phi(0, N_j)\Phi(\ell, L_n), \qquad (26)$$

$$P[\beta_n = 1, k_n = \ell] = \Phi(\ell, L_n) - P[\beta_n = 0, k_n = \ell]. \qquad (27)$$

The joint probability distribution $P[\beta_n, k_n]$, $1 \le n \le N$, allows for the evaluation of several performance measures of interest at the AAL2, such as the mini-Cell Loss Rate ($mCLR$) defined as the probability that a CPS packet is lost, due to uncorrectable errors in the ATM header, in the STF or in the CPS Packet's header. The $mCLR$ can be used to evaluate improved ATM/AAL2 header protection schemes. The mini-Cell Loss Rate for CPS packet n is given by

$$mCLR_n = \sum_{\ell=0}^{L_n} P[\beta_n = 1, k_n = \ell]$$
$$= P[\beta_n = 1] = 1 - P[\beta_n = 0], \qquad (28)$$

where L_n is the size of the payload of CPS packet n.

Also of interest is the *mini-cell Payload Error Rate (mPER)* defined here as the BER of the CPS Packets delivered by the AAL2 to higher layers. That is, *mPER* is the average number of errors in the CPS packet payload given that header/control fields that affect the delivery of the CPS packet payload to higher layers are correct. The *mPER* provides information regarding the impact of errors on the payload of AAL2 CPS Packets. The mini-cell Payload Error Rate for CPS packet n is given by

$$mPER_n = \frac{\sum_{\ell=0}^{L_n} \ell \cdot P[\beta_n = 0, k_n = \ell]}{L_n \sum_{\ell=0}^{L_n} P[\beta_n = 0, k_n = \ell]}.$$ (29)

Finally, the *mini-cell Payload Bit Error Rate (mPBER)* is defined as the BER seen by higher layers, as a result of bit errors in the payload of undiscarded CPS Packets and lost bits due to the discard of CPS Packets. The *mPBER* provides an overall picture of the BER seen by higher layers as it evaluates the combined effect of the impact of errors on headers and payload. Hence *mPBER* can be used to evaluate the QoS requirements for the users of the AAL2. The mini-cell Payload Bit Error Rate for CPS packet n is given by

$$\begin{aligned} mPBER_n &= \sum_{\ell=0}^{L_n} \left[P[\beta_n = 1, k_n = \ell] + \frac{\ell}{L_n} P[\beta_n = 0, k_n = \ell] \right] \\ &= mCLR_n + \sum_{\ell=0}^{L_n} \left[\frac{\ell}{L_n} P[\beta_n = 0, k_n = \ell] \right]. \end{aligned}$$ (30)

7.2 Performance Results over the Gilbert-Elliott Channel

Numerical results for performance measures *mCLR*, *mPER* and *mPBER*, derived in Equations (28)-(30) are presented in this section. The CPS-PDU structure shown in Figure 20 is considered for the derivation of numerical results ($M = 0$) with the assumption that the CPS Packets are of equal size. The BER for the Gilbert-Elliott channel model is $\varepsilon = 10^{-3}$ with $P_e(0) = 0$ and $P_e(1) = 0.5$.
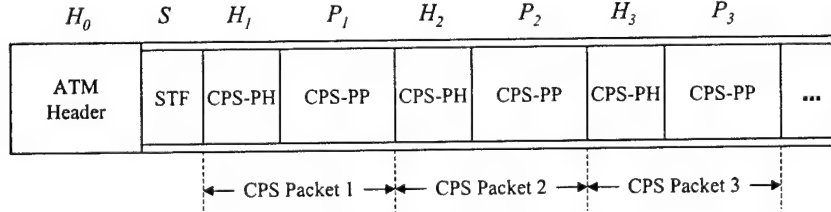
Figure 20: CPS-PDU structure.

Results for the three performance measures for CPS packet 1 with payload size $L_1 = 96$ bits (12 bytes) are shown in Figure 21.
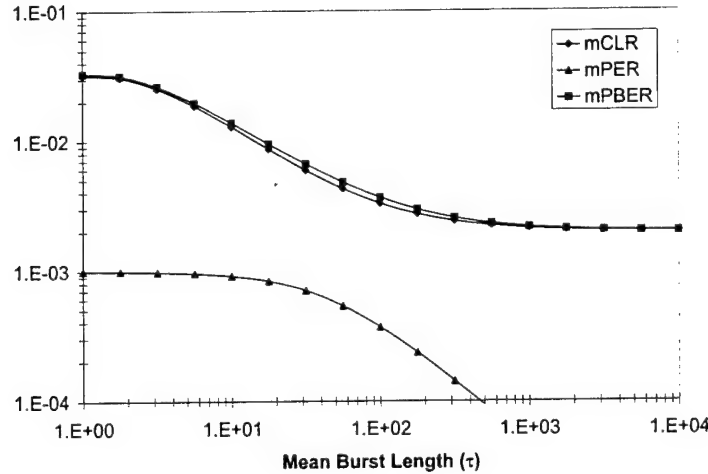
Figure 21: Results for mCLR, mPBER and mPER versus τ for CPS packet 1.

It is clear that the error performance with respect to all measures improves as the mean burst length τ increases. As the value of τ increases ($\tau \to \infty$), *mCLR* and *mPBER* approach a limit, which can be shown to be equal to

$$mCLR(\infty) = 1 - \pi_0 - \pi_1 \left\{ [1 - P_e(1)]^{N_0} + N_0 P_e(1)[1 - P_e(1)]^{N_0-1} \right\} [1 - P_e(1)]^{N_S+N_1},$$ (31)

while *mPER* continues to decrease monotonically. This performance behaviour is attributed to the analytical model used for the channel as explained below. For large values of τ, the error process

consists of long bursts of errors, followed by long error-free periods. As the mean burst length decreases with τ and for a fixed BER, the length of error-free periods must also decrease with τ. That is, for small values of τ, the error process consists of relatively short error bursts and error-free periods. An illustrative example of the error process for large and small values of τ is shown in Figure 22.

For small values of τ, the ATM/AAL2 bit stream is affected by short and frequent error bursts, and in consequence, the probability of a header/control field being corrupted by errors, i.e. the *mCLR*, increases. Therefore, the *mCLR* performance degrades as τ decreases. For long error bursts spanning several ATM cells (large τ), the discarded CPS Packets will have all payload bits in error. Similarly, CPS Packets that are not discarded will likely have error-free payloads. So, for large values of τ, the payload of a CPS packet delivered to the higher layers is more likely to be free of errors, and *mPER* decreases with τ. Note that the *mPBER* is only slightly higher than *mCLR* (Figure 21). From this observation it is clear that the main factor contributing to the BER seen by the higher layer (*mPBER*) is the *mCLR*, more specifically, the payload errors due to CPS Packets being discarded. Recall that, from the definition of *mPBER*, bits lost at the ATM/AAL2 are considered bit errors at the higher protocol layers.

Performance measures for a CPS packet depend on the position of the packet in the CPS-PDU payload. Figure 23 shows the results for *mCLR* as a function of the mean burst length τ for CPS Packets 1, 2 and 3 ($L_1 = L_2 = L_3 = 96$ bits). In addition, Figure 24 and Figure 25 show the results for *mPBER* and *mPER*, respectively.
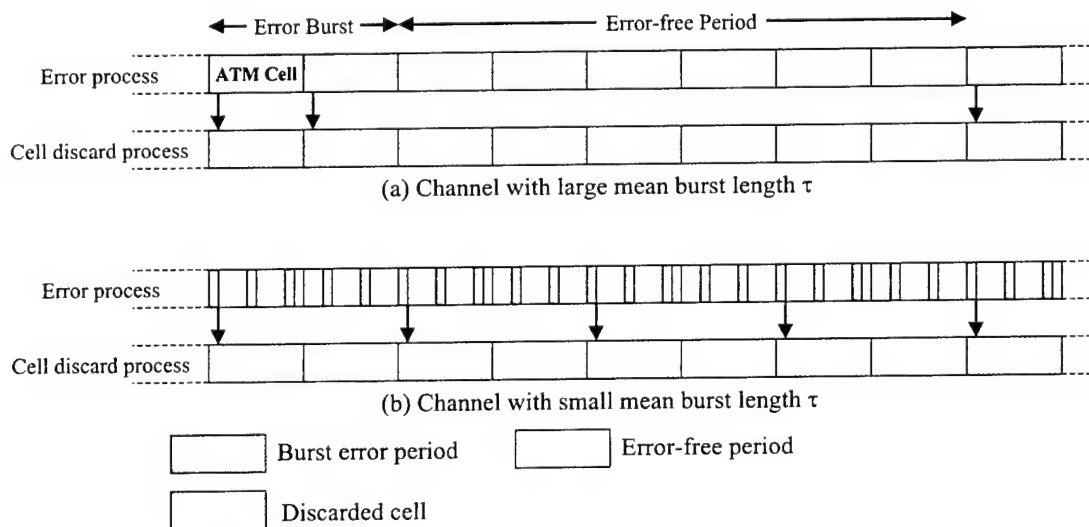
Figure 22: Burst error process.
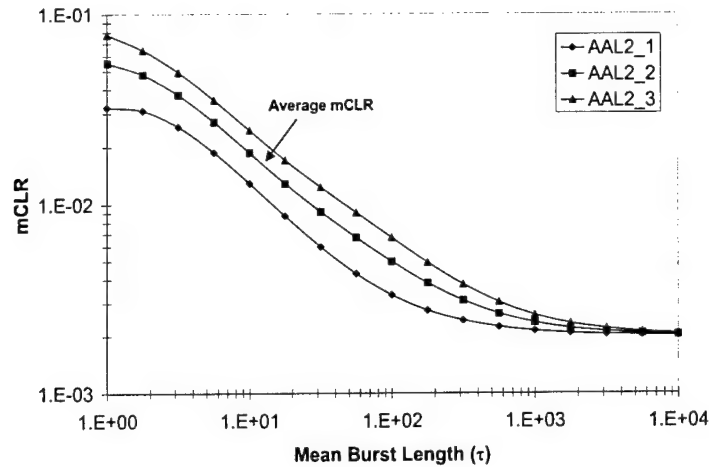
Figure 23: Results for mCLR versus τ for CPS packets 1, 2 and 3.

From Figure 23 it is clear that the *mCLR* performance is best for CPS packet 1 and degrades with each subsequent CPS packet in the CPS-PDU payload. This behaviour is explained in view of the fact that the successful delivery of the CPS packet to the higher layers requires that the header of the CPS packet be correct, and in addition, that all headers from previous CPS Packets in the CPS-PDU payload be correct.

It should be noted that under the current definition of AAL2, users of the AAL2 do not have predetermined positions within the CPS-PDU payload, and therefore, no single user will be adversely affected by having its packets permanently assigned the last position in the CPS-PDU payload. Results for the average *mCLR* over all CPS packets in the CPS-PDU payload are shown in Figure 23, where the curve for the average *mCLR* coincides with the curve for the *mCLR* for CPS packet 2. Similar results are obtained for the average *mPBER* shown in Figure 24.
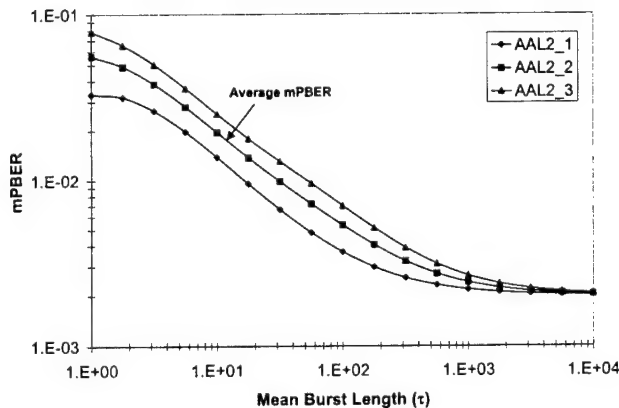

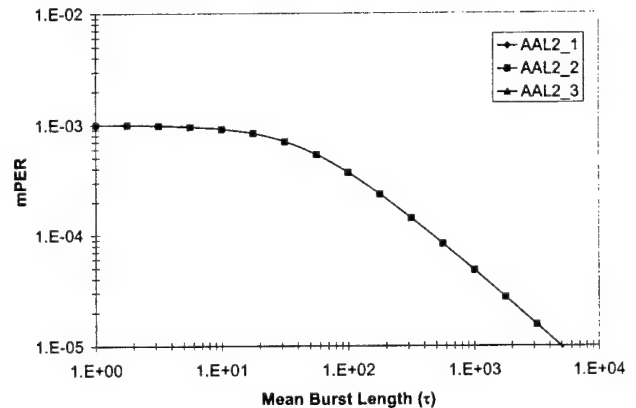*Figure 24: Results for mPBER versus τ for CPS packets 1, 2 and 3.*

Figure 25: Results for mPER versus τ for CPS packets 1, 2 and 3.

27

It is important to recall that a CPS packet can be mapped across CPS-PDU payload boundaries; in this case, the CPS packet is split in two parts, which are transported, by two separate ATM cells. Performance measures for this scenario are not addressed in this study, but the results are expected to be worse than those in the case where a CPS packet is transported in a single ATM cell, as the successful delivery of the CPS packet requires the correctness of two rather than one ATM cell headers. Results for the *mPER* are shown in Figure 25. All three CPS Packets in the CPS-PDU payload have the same *mPER*. This is due to the fact that all CPS Packets have the same payload size; hence given there are no errors in the header/control fields, the BER of the payload is the same for all CPS Packets.

Since ATM Adaptation Layer 2 can accommodate CPS Packets of variable payload sizes, it is of interest to study the performance of AAL2 over the burst error channel for CPS Packets with different payload sizes. For this purpose, numerical results for CPS Packets with payload size equal to 24, 96 and 352 bits are presented in Figure 26 - Figure 28. The results shown in these figures represent the average values over all CPS Packets that are carried in the CPS-PDU payload. The CPS-PDU payload carries 7, 3 or 1 complete CPS Packets for payloads of size 24, 96 or 352, respectively.
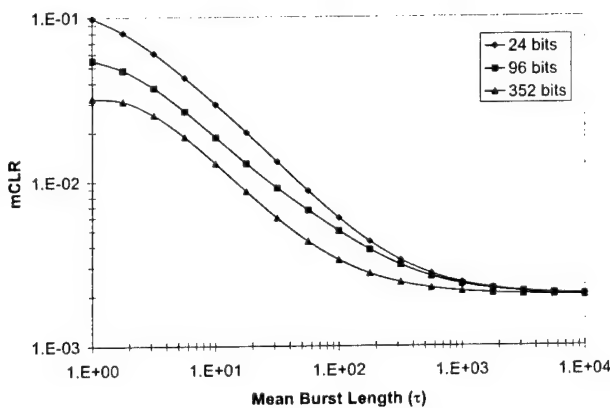
Figure 26: Results for mCLR versus τ for different CPS packet payload sizes.
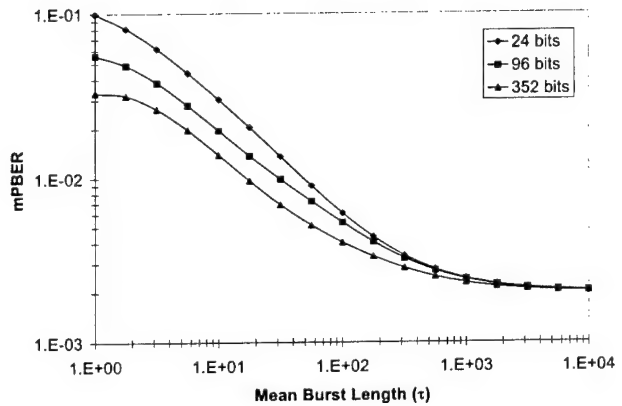
Figure 27: Results for mPBER versus τ for different CPS packet payload sizes.

From Figure 26 and Figure 27 it is observed that performance with respect to *mCLR* and *mPBER* improves for large CPS packet payloads. For large CPS packet payloads the number of CPS Packets that are carried in the CPS-PDU decreases and so does the number of CPS packet headers, thus the probability of corrupted headers affecting CPS packet delineation and resulting in CPS packet loss decreases.

Figure 28 shows *mPER* for CPS Packets of different payload sizes. Contrary to the behaviour exhibited by *mCLR* and *mPBER*, the performance with respect to *mPER* improves for CPS Packets with small payload sizes. By definition, *mPER* is associated with the rate of errors in the CPS packet payloads given that the header/control fields are correct, and thus, depends on the effect of the error process on the CPS packet payload only. The probability of errors in the CPS packet payload increases with the size of the payload.

28

From these results it is clear that a system implementation using large CPS packet payloads will result in a reduced *mCLR* at the expense of increased *mPER* and packetization delay.
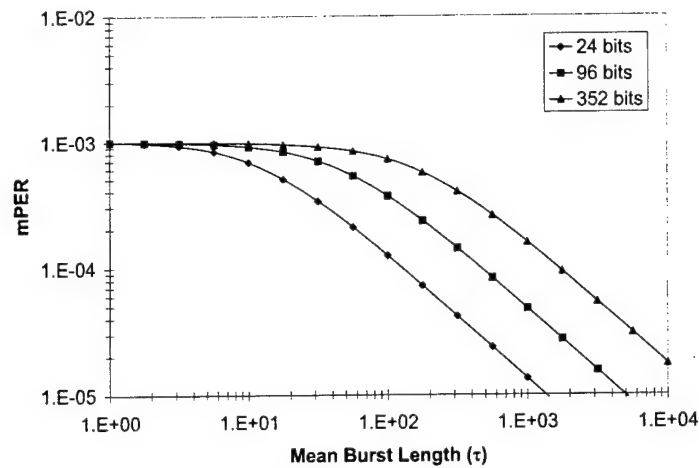
Figure 28: Results for mPER versus τ for different CPS packet payload sizes.

Remarks:

- Numerical results presented in this section demonstrate that the BER seen by the layer above the AAL2 is greatly due to the impact of bit errors over ATM/AAL2 headers, as it is shown by performance measures *mCLR* and *mPBER*. This clearly indicates the need for an improved method for the protection of ATM/AAL2 header fields.

- It has also been shown that performance results depend on the relative position of the AAL2 CPS packet within the payload of the CPS-PDU. In this way, the first AAL2 Packet that appears immediately after the STF field shows the best performance in terms of measure *mCLR* (probability of the AAL2 CPS packet being discarded due to errors in ATM/AAL2 header fields).

- In addition, it has been found that the use of large size AAL2 CPS Packets is preferable for the transport over wireless channels at the expense of increased packetization delays and payload BER.

7.3 Performance Results for AAL2 with BCH Encoded Headers

Channel coding protects digital data from errors by selectively introducing redundancies in the transmitted data. Channel codes that are used to detect errors are called error detection codes, while codes that can detect and correct errors are called error correction codes. A channel coder operates on digital messages (or source) data by encoding the source information into a code sequence for transmission through the channel. There are two basic types of error correction and detection codes: *block codes* and *convolutional codes*. In this work we demonstrate the performance that is achieved by implementing block codes to protect the frame structure of ATM/AAL2. The use of convolutional codes is not addressed in this work, as block codes are better suited for the protection of block structured data, such as ATM cells.

Block codes are Forward Error Correction (FEC) codes that enable a limited number of errors to be detected and corrected without retransmission. Block codes are used to improve the performance of a communications system when other means of improvement (such as increasing transmitter power or using a more sophisticated demodulator) are impractical. In block codes, parity bits are added to blocks of message bits to make *codewords* or *code blocks*. In a block encoder, k information bits are encoded into n code bits. A total of $(n - k)$ redundant bits are added to the k information bits for the purpose of detecting and correcting errors. The block code is referred to as an (n, k) code, and the rate of the code is defined as $R_c = k/n$ and is equal to the rate of information divided by the raw channel rate.

Several schemes are foreseen to implement the usage of a forward error correction code within an ATM cell. Some of these schemes apply a FEC code to the entire ATM cell (header and payload) or to the ATM header independently of the ATM payload. The first method results in an inefficient use of the FEC code, as the header and payload are given the same amount of protection. In the latter method a stronger FEC code is applied to the ATM header and upon the application requirements a FEC code can be applied to the ATM payload. Further more, once a FEC code has been applied to the header, these bits can be interleaved with the payload bits to protect the header information from burst errors.

In this section, numerical results are presented to demonstrate the performance of ATM/AAL2 by implementing block codes to protect the headers of the ATM/AAL2 frame structure. For the purpose of analysis, three scenarios are considered:

1. The HEC field, from the standard ATM header, is replaced by a BCH code to protect the ATM header.

2. The HEC field, from the standard ATM header, is removed and a BCH code is used to protect the remaining 4 header octets, plus the single octet STF field (only 7 bits are encoded from the STF field, as the bit used for parity is removed).

3. The HEC field, from the standard ATM header, is removed and a BCH code is used to protect the remaining 4 header octets, plus the single octet STF field. In addition, the HEC field from the AAL2 CPS packet is replaced by a BCH code to protect the AAL2 CPS packet header.

7.3.1 BCH Encoded ATM Header

This scenario is used to demonstrate the use of a BCH code, which replaces the single octet HEC field that is used to protect the header of the ATM cell. In this way, the remaining 4 header octets (32 bits) are encoded using the shortened codes BCH(44,32), BCH(50,32), BCH(56,32) and BCH(59,32), which are capable of correcting up to $t = 2$, 3, 4 and 5 bits in error respectively.

Numerical results for performance measures $mCLR$, $mPER$ and $mPBER$, derived in Equations (28)-(30) are presented in this section. The CPS-PDU structure shown in Figure 29 is considered for the derivation of numerical results ($M = 0$) and CPS Packets are assumed to be of equal size (CPS packet payload size of 96 bits). The BER for the Gilbert-Elliott channel model is $\varepsilon = 10^{-3}$ with $P_e(0) = 0$ and $P_e(1) = 0.5$.
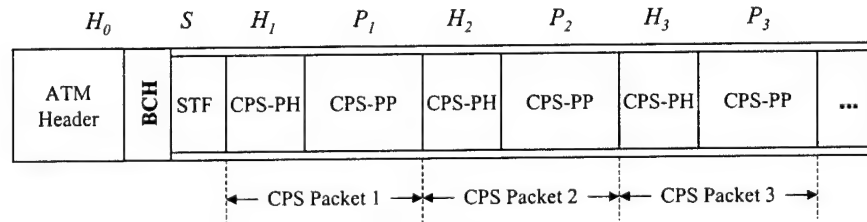

Figure 29: BCH encoded ATM header

Results presented in Figure 30 - Figure 32 correspond to the performance of CPS packet 1, as it is shown in Figure 29. For comparison purposes, performance results obtained under the standard ATM/AAL2 frame structure are also presented in these figures and are denoted under the HEC label.

From Figure 30 it is observed that performance improvements for metric $mCLR$ are small and only noticeable for relatively small mean burst lengths, $\tau < 10$ bits, as BCH encoded header are capable of correcting some of the ATM header errors. This is a result of the limited error correcting capability of the BCH encoded headers. On the other hand, for mean burst lengths greater than 10 bits, $\tau > 10$, the error correcting capability of the BCH codes is far exceeded, thus performance remains the same for all the different code rates.

Performance results for metric $mPBER$ are presented in Figure 31. It should be noted that performance results obtained for this metric are similar to the results of metric $mCLR$, presented in Figure 30. This is explained in terms of the definition of $mPBER$, which is the BER experienced by the layers above the AAL and it is given by Equation 30. From Equation 30 it is clear that the $mPBER$ is a function of the $mCLR$ plus the average of bit errors in the payload of non-discarded AAL2 packets. Therefore, the results presented in Figure 31 imply that the BER experienced by the layers above the AAL2 is greatly due to the impact of lost AAL2 Packets.

Figure 32 shows the results for performance metric $mPER$. From this figure it is observed that the performance remains the same for all the protection schemes. This result is expected, as metric $mPER$ reflects the average BER on the payload of non-discarded AAL2 packets. Consequently, the BER should remain unaffected as none of the analysed scenarios provide any correction capability for the payload of AAL2 CPS Packets.

Figure 30: mCLR results for BCH encoded ATM header.
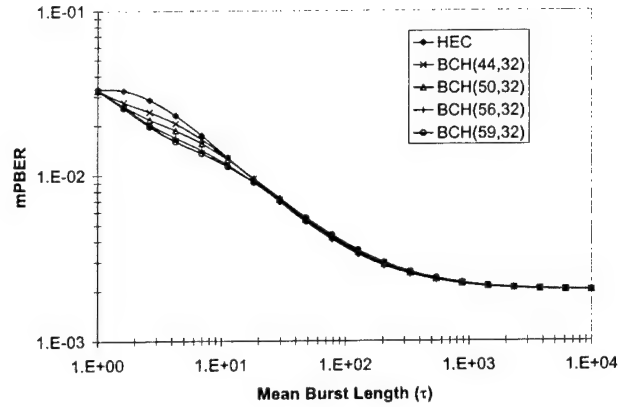
Figure 31: mPBER results for BCH encoded ATM header.
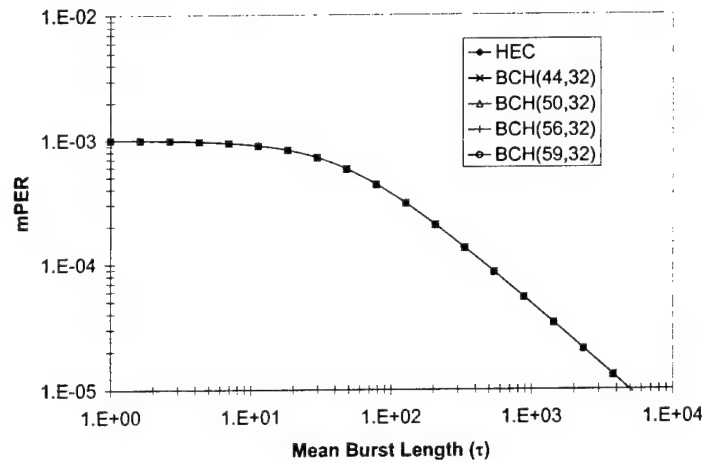
Figure 32: mPER results for BCH encoded ATM header.

7.3.2 BCH Encoded ATM/STF Headers

This scenario is presented to demonstrate the use of a BCH code to protect the first 4 octets of the ATM header, plus the STF field. In this way, the ATM header and the STF field (the combined size of the ATM header plus the STF field is 39 bits) are encoded using the shortened codes BCH(51,39), BCH(57,39), BCH(63,39) and BCH(74,39), which are capable of correcting up to $t = 2, 3, 4$ and 5 bits in error respectively.

The CPS-PDU structure shown in Figure 33 is considered for the derivation of numerical results ($M = 0$) and CPS Packets are assumed to be of equal size (CPS packet payload size is 96 bits). The BER for the Gilbert-Elliott channel model is $\varepsilon = 10^{-3}$ with $P_e(0) = 0$ and $P_e(1) = 0.5$.

Figure 33: BCH encoded ATM/STF headers

From the performance results shown in Figure 34 - Figure 36, it is observed that performance improvements are not noticeable compare to the results presented in section 7.3.1. The main difference is only observable for the results of metrics *mCLR* and *mPBER* for a mean burst length of 1 bit, $\tau = 1$, and is explained by the fact that the STF field is protected along with the ATM header, thus providing a slight improvement.
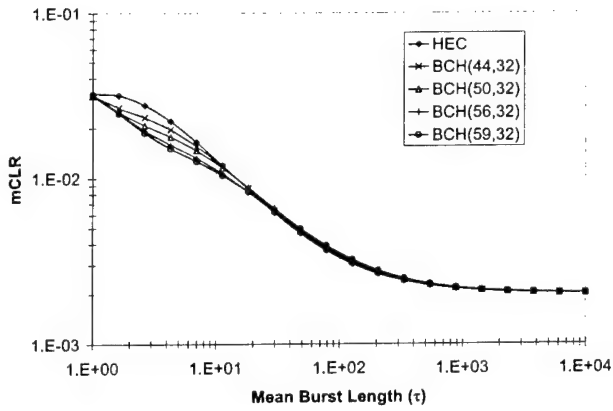

Figure 34: mCLR results for BCH encoded ATM/STF headers.

Figure 35: mPBER results for BCH encoded ATM/STF headers.

Figure 36: mPER results for BCH encoded ATM/STF headers.

33

7.3.3   BCH Encoded ATM/STF/AAL2 Headers

The CPS-PDU structure shown in Figure 37 is considered for the derivation of numerical results ($M = 0$) and the CPS packets are assumed to be of equal size (CPS packet payload size is 96 bits). The BER for the Gilbert-Elliott channel model is $\varepsilon = 10^{-3}$ with $P_e(0) = 0$ and $P_e(1) = 0.5$.
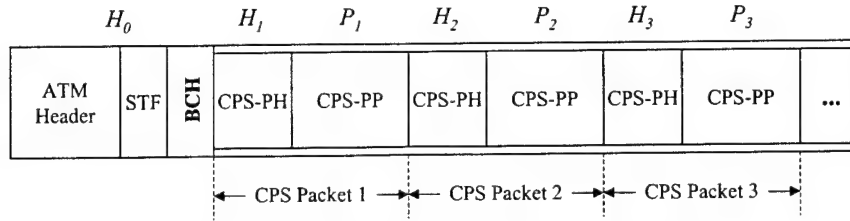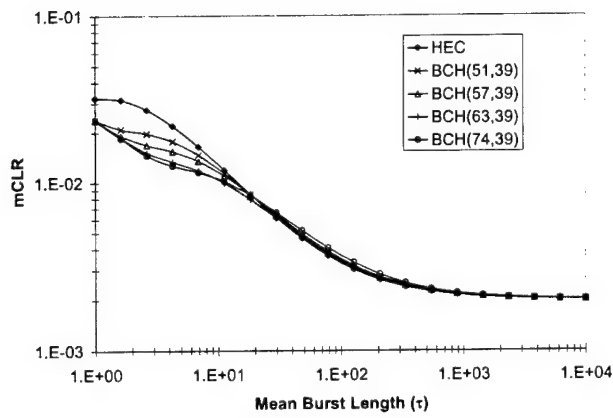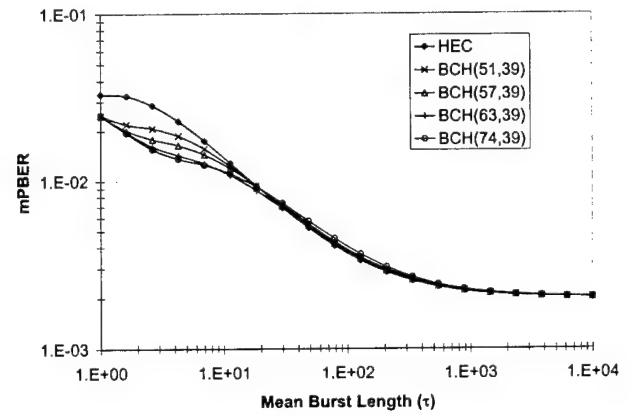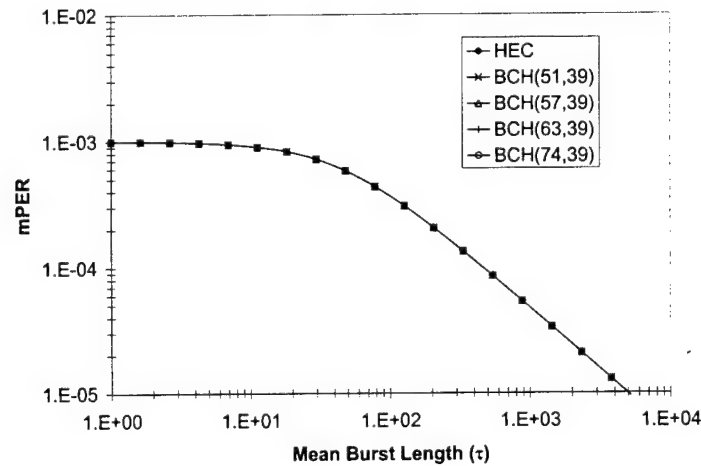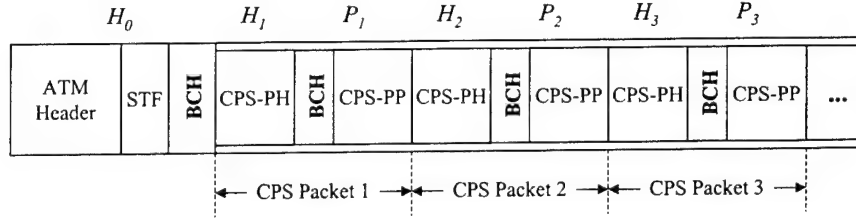

Figure 37: BCH encoded ATM/STF/AAL2 headers

The scenario presented in this section is divided in two groups, where a different code rate is used to protect the header of the AAL2 Packet.

- *AAL2 CPS packet header protected with shortened BCH(24,19)*

This scenario demonstrates the use of a BCH code to protect the first 4 octets of the ATM header, plus the STF field. In this way, the ATM header and the STF field (the combined size of the ATM header plus the STF field is 39 bits) are encoded using the shortened codes BCH(51,39), BCH(57,39), BCH(63,39) and BCH(74,39), which are capable of correcting up to $t = 2, 3, 4$ and 5 bits in error respectively. In addition the AAL2 CPS packet header is encoded by a shortened BCH(24,19) code with correcting capability $t = 1$ bit.

Figure 38, shows performance results for metric *mCLR*. From these results it is observed that performance is improved for mean burst lengths smaller than 2 bits, $\tau \leq 2$, compared to the results presented in sections 7.3.1 and 7.3.2. In particular, for $\tau = 1$ metric *mCLR* is approximately 2.5×10^{-4}. Similarly, performance results for metric *mPBER* also present an improvement for small mean burst lengths, $\tau \leq 2$. An interesting observation is that metric *mPBER*, shown in Figure 39, no longer follows metric *mCLR* for mean burst lengths smaller than 2 bits, $\tau \leq 2$. This observation is explained by the fact that the probability of a lost AAL2 packet is smaller than the probability of errors on the payload of non-discarded AAL2 packets, consequently for $\tau \leq 2$, the contributing factor over metric *mPBER* is the probability of errors on the payload of non-discarded AAL2 CPS Packets, as information bits carried in the AAL2 CPS-PP are not protected against bit errors.

Figure 40 shows performance results for metric *mPER*. Numerical results for this metric remain unaffected compared to the same results presented in sections 7.3.1 and 7.3.2. This result is explained by the fact that none of these scenarios provide any protection for the payload of AAL2 packets and therefore the probability of corrupted bits over the payload remains the same for all analysed scenarios.

Figure 38: mCLR results for BCH encoded ATM/STF/AAL2 headers.

Figure 39: mPBER results for BCH encoded ATM/STF/AAL2 headers.
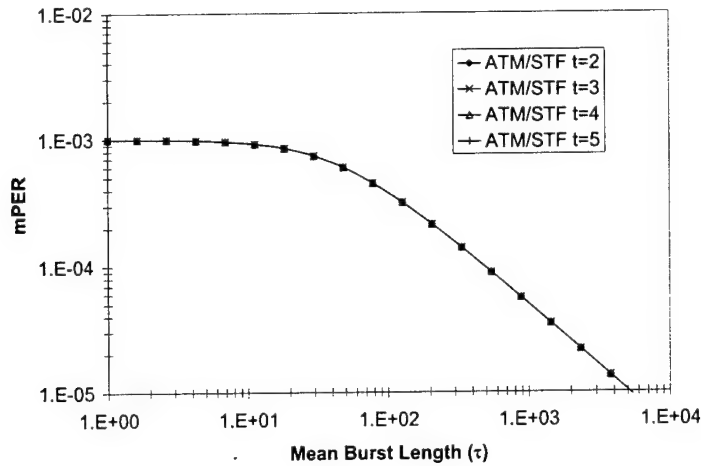
Figure 40: mPER results for BCH encoded ATM/STF/AAL2 headers.

- *AAL2 CPS packet header protected with shortened BCH(29,19)*

This scenario evaluates the use of a BCH code to protect the first 4 octets of the ATM header, plus the STF field. In this way, the ATM header and the STF field (the combined size of the ATM header plus the STF field is 39 bits) are encoded using the shortened codes BCH(51,39), BCH(57,39), BCH(63,39) and BCH(74,39), which are capable of correcting up to t = 2, 3, 4 and 5 bits in error respectively. In addition the AAL2 CPS packet header is encoded by a shortened BCH(29,19) code with correcting capability t = 2 bits.

From the results presented in Figure 41 - Figure 43 we derive the same conclusions presented for the previous scenario (AAL2 packet with BCH encoded header with correcting capability of t = 1 bit). The main differences, under this scenario, are the results presented for metric $mCLR$. In particular for a mean burst length of τ = 1 bit, where $mCLR$ is reduced to approximately 3.5×10^{-5}. However, the BER experienced by the layer above the AAL does not benefit by the improvement over $mCLR$ (for τ = 1) as the BER over the payload of non-discarded AAL2 packets remains the main factor contributing to the performance of $mPBER$.
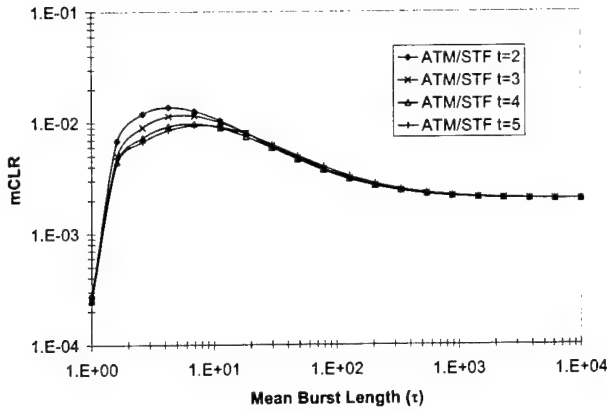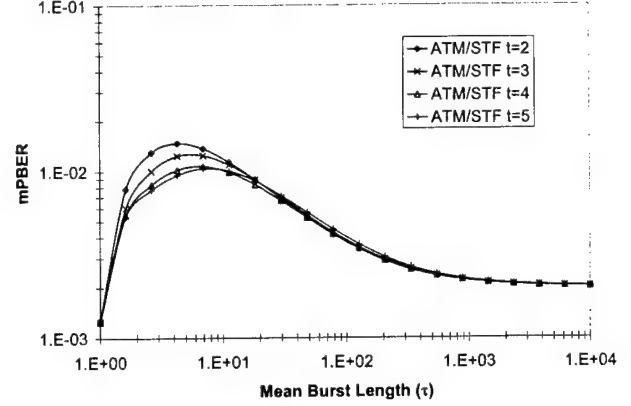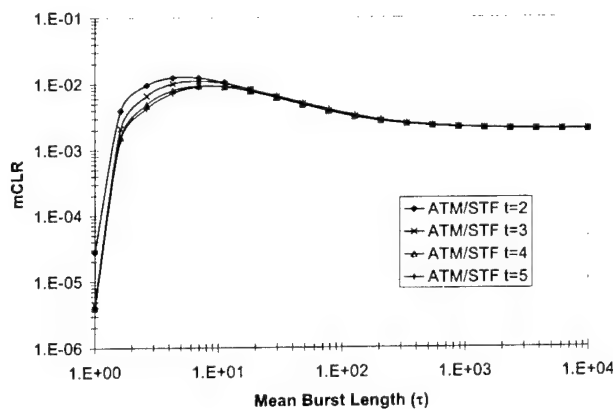
Figure 41: mCLR results for BCH encoded ATM/STF/AAL2 headers.
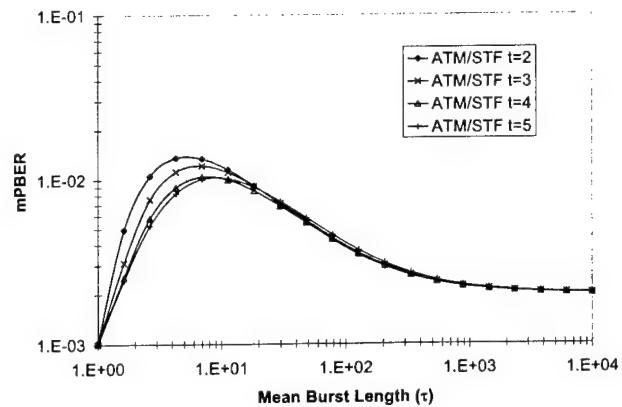
Figure 42: mPBER results for BCH encoded ATM/STF/AAL2 headers.
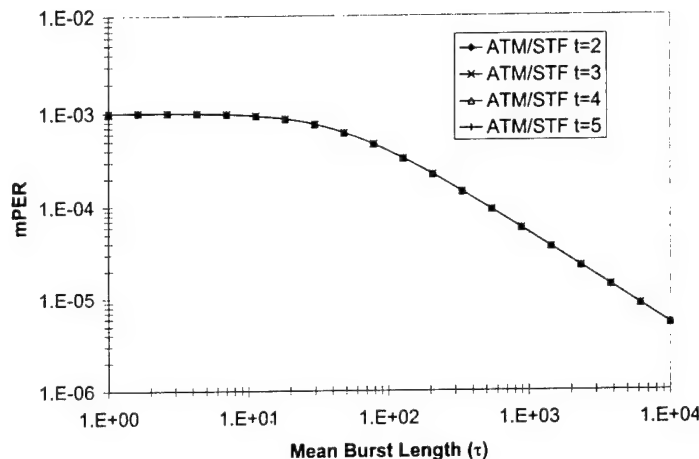
Figure 43: mPER results for BCH encoded ATM/STF/AAL2 headers.

Remarks:

- Numerical results presented in this section indicate that the use of BCH for the protection of the ATM and the STF fields do not provide for any additional benefit over the performance results obtained under the standard ATM/AAL2 frame structure.

- Significant performance gains over metric *mCLR* are observed for the case in which the AAL2 packet header is protected by a BCH code, in addition to the BCH encoded ATM header and STF field. However, these gains are only significant for small mean burst lengths in the order of 1 bit, $\tau \approx 1$. As the code rate for the BCH code used to protect the AAL2 is reduced, thus increasing the error correcting capability of the code, the *mCLR* metric is also reduced. However, further improvements achieved over metric *mCLR* are not reflected over the BER experienced by the layers above the AAL2 (i.e. metric *mPBER*), as payload bits are now the main source of bit errors contributing to the impact over metric *mPBER*.

36

7.4 Improved Delineation Mechanism for AAL2

Identifying the need for a new ATM Adaptation Layer (AAL), which could efficiently support low data rate and delay sensitive applications, the ITU-T has standardized the AAL Type 2 (AAL2) under specification I.363.2 [2]. One of the main characteristics of AAL2 is that it improves bandwidth utilization by multiplexing low data rate and delay sensitive traffic from multiple sources into a single ATM virtual circuit. Nevertheless, as currently specified, AAL2 does not perform very efficiently under high bit error rate links. One of the reasons for the poor performance of AAL2 is due to the way packets are delineated within the ATM payload. In this Section a novel mechanism is presented for the delineation of CPS Packets to allow for improved performance over high BER links. In addition the proposed mechanism reduces the required overhead, due to delineation fields, while preserving interoperability with standard AAL2.

7.4.1 Delineation over Standard AAL2

AAL2 achieves efficient bandwidth utilization by multiplexing data from multiple sources within the payload of the AAL2 Common Part Sublayer Protocol Data Unit (CPS-PDU). The CPS-PDU consists of a single byte start field, STF, and a 47-byte payload. The CPS-PDU payload may carry zero, one or more (complete or partial) CPS Packets. Each CPS packet is composed by a three byte Common Part Sublayer Packet Header (CPS-PH) and a variable size Common Part Sublayer Packet Payload (CPS-PP) [2], as shown in Figure 44.
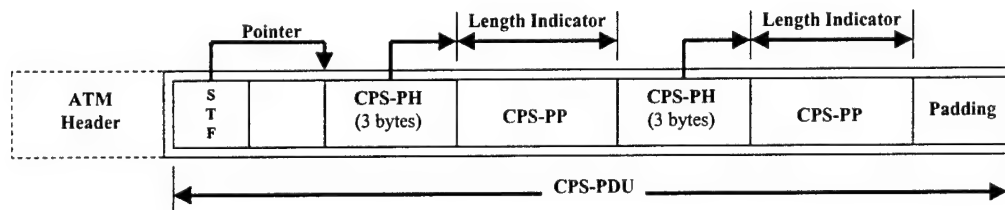
Figure 44: CPS packet delineation over standard AAL2.

Under AAL2, CPS packet delineation is achieved by identifying the position of the first CPS packet in the CPS-PDU payload and then deriving the position of each subsequent CPS Packet. To this matter, the STF field contains the required information to identify the position of the first CPS Packet, while the Length Indicator (LI) field in each CPS-PH is used to derive the position of each subsequent CPS packet within the CPS-PDU payload, as depicted in Figure 44.

From the delineation mechanism implemented for standard AAL2 it is possible to make the following observations:

- There is an inherent dependency between CPS Packets carried within the CPS-PDU payload, due to the delineation mechanism. That is, for a CPS packet not to be discarded, it is required that its CPS-PH be correct, in addition to any previous header fields required to preserve delineation within the CPS-PDU payload. For example, the first CPS packet relies on the ATM header, the *STF* and its own CPS-PH field being correct for the CPS packet not to be

discarded at the ATM or AAL2 layer. On the other hand, the second CPS packet will have to rely on the same three previous header fields, as the first CPS Packet, in addition to its own CPS-PH field.

- Another interesting observation is that the delineation field within the CPS-PH, namely the *LI*, is formed by a sequence of 6 bits. However, delineation is lost not only if any of these 6 bits are corrupted by errors, but also if there are errors affecting the rest of the CPS-PH, which is 3 bytes long. Thus, the probability of losing delineation within the CPS-PDU payload becomes a function of the probability of errors corrupting the entire CPS-PH field and not only the *LI* field.

7.4.2 Improved Delineation Mechanism

The proposed delineation mechanism is implemented by introducing a new Delineation Field (*DF*), which replaces the functionality provided by the *STF* and *LI* fields. Figure 45 depicts the process by which the new delineation field is created.
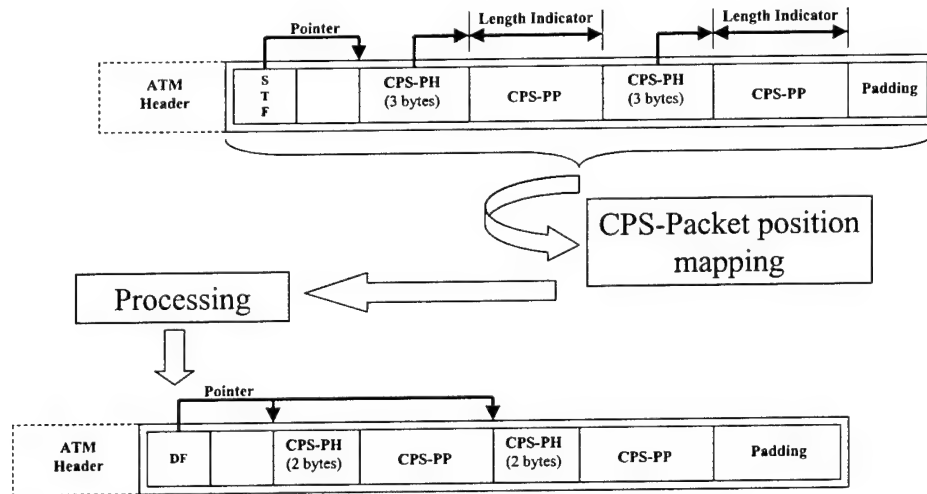
Figure 45: Delineation mechanism process.

The CPS-PDU is represented by a sequence $S_i = \{x_1, x_2,..., x_{48}\}$ of 48 bits (6 bytes), where $i = 1$, $2,..., N$ and N is equal to the number of possible combinations of S_i. Furthermore, there is a one-to-one correspondence from each of the 48 bytes from the CPS-PDU to each element x_k, $k = 1, 2,..., 48$, as depicted in Figure 46. By definition, all elements x_k are equal to zero, except for those elements that are mapped from the CPS-PDU and correspond to the beginning of a CPS-Packet, in this case, element x_k will be equal to one. Thus, sequence S_i is composed of elements $x_k \in \{0,1\}$.
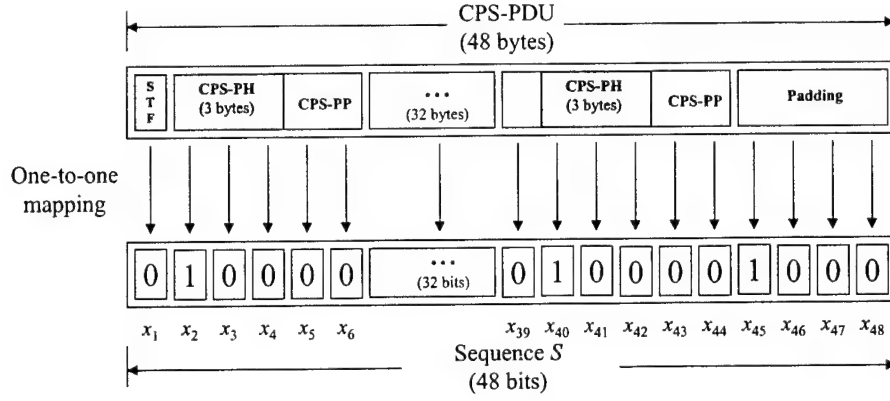
Figure 46: Delineation sequence mapping.

Due to the structure of a CPS-PDU, not all possible vectors $\{x_1, x_2,..., x_{48}\}$ correspond to a valid combination of sequence S_i. For example, x_1 is always equal to 0 because the first byte in the CPS-PDU is allocated to the *STF* field. Furthermore, if $x_k = 1$ for any $2 \le k \le 48$, then x_{k+1}, x_{k+2} and x_{k+3} are equal to zero because each CPS packet is at least 4 bytes long; it consists of a 3 byte CPS-PH and a CPS packet payload that is at least one byte long. In general, let m be the total number of bits in sequence S_i. Since the smallest possible CPS packet is 4 bytes long, the maximum possible number of *complete* CPS Packets in a CPS-PDU is given by $n = \lfloor m / 4 \rfloor$, where $\lfloor x \rfloor$ is the largest integer smaller than x. Then, the number of possible combinations of S_i is given by,

$$\Psi(m,n) = \sum_{i=1}^{n}\left[\binom{m-3i}{i} + \sum_{j=m-3}^{m-1}\binom{j-3(i-1)}{i-1}\right] + \sum_{k=1}^{m-4n}\binom{(m-k)-3n}{n} + 1. \tag{32}$$

For AAL2, it follows that element x_1 is always equal to zero, as it corresponds to the *STF*, so $m = 48 - 1 = 47$ and the number of possible combinations, of sequence S_i is $N = \Psi(47, 11)$. Due to the high redundancy of data in sequence S_i (i.e. the number of elements x_k equal to zero is always greater than that of x_k equal to one) it is possible to introduce compression, which becomes the last *processing* step in creating the Delineation Field, *DF*.

The compression of delineation sequence, S_i, is achieved by introducing the concept of a delineation matrix **D**. The 48 elements of vector $\{x_1, x_2, \dots, x_{48}\}$ are mapped into elements, d_{ij}, $i=1,2,\dots,r$ and $j=1,2,\dots,c$, of matrix **D** with r rows, c columns and $r \cdot c \ge 48$. Starting with x_1, matrix **D** is filled one row at a time, thus $d_{ij} = x_k$ following

$$i = \lceil k/c \rceil, \quad j = k - c(i-1) \ \forall \ k = 1, 2, \dots, 48, \tag{33}$$

where $\lceil x \rceil$ is the smallest integer that is greater than x.

The selection of an appropriate matrix **D** of order $r \times c$ should include integer numbers, such that, $r \cdot c = 48$ and $r, c \notin \{1, 48\}$, for example $r, c \in \{2, 3, 4, 6, 8, 12, 16, 24\}$. For a given matrix **D**, sequence R_j is defined as the sequence of bits, $R_j = \{y_1, y_2,..., y_c\}$ for $j = 1, 2,..., N_y$, that corresponds

to a valid row vector. N_y is equal to the number of possible combinations of R_j, in sample space **R**, and c is the total number of columns. In addition, sequence L_k is defined as the sequence of bits that form row vector k, that is, $L_k = \{d_{k1}, d_{k2}, ..., d_{kc}\}$ for $k = 1, 2, ..., r$. From the previous definitions, it should be clear that $\{L_k\}_{k=1,2,...,r} \in \mathbf{R}$. For AAL2, the number of valid combinations of $\{R_j\}_{j=1, 2,..., Ny}$ is given by,

$$N_y = \Psi(c, \lfloor c / 4 \rfloor). \tag{34}$$

Given a matrix **D**, compression is used over all row sequences $\{R_j\}_{j=1,2,...,Ny}$ by implementing Huffman coding. Thus, for each row sequence $\{L_k\}_{k=1,2,...,r}$ in matrix **D**, there is a Huffman code associated to it, as $\{L_k\}_{k=1,2,...,r} \in \mathbf{R}$. The sequence of bits from the Huffman codes associated to $\{L_k\}_{k=1,2,...,r}$ are used to form the Delineation Sequence, DS, that is part of the Delineation Field, DF.

7.4.3 Delineation Mechanism in AAL2

The introduction of the delineation field, DF, in AAL2 will result in the removal of the STF and LIs fields from the CPS-PDU. The removal of the LI field (6 bits) from the CPS-PH results in a CPS-PH of size 18 bits, which is not a multiple of eight. Thus, in addition to the removal of the LI field, it is further required that two additional bits be removed from the CPS-PH. It is proposed that the HEC field contain the remainder of the division (modulo 2), by the generator polynomial X^3+X+1, of the product of X^3 and the contents of the first 13 bits of the CPS-PH. In this way, the HEC field will require 3 bits and therefore the resulting CPS-PH will further be reduced to a more suitable size of 16 bits (2 bytes).

Table 2: Huffman codes size for R_i.

Matrix D	N_y	Max. Huffman Codes Size (bits)
24 × 2	3	2
16 × 3	4	3
12 × 4	5	3
8 × 6	10	5
6 × 8	19	6
4 × 12	69	8
3 × 16	250	9
2 × 24	3292	13

Under the constrain that the resulting DF field should be as short as possible, Huffman coding is used to compress vector sequences R_j. This is done by assuming a very high probability of occurrence for the vector sequence R_j with elements all equal to zero, so the resulting Huffman code will be of size 1-bit. A uniform probability of occurrence is assumed for the rest of possible combinations of sequence R_j. Table 2 shows the size of the largest resulting Huffman codes for different dimensions of matrix **D**.

Let N_r be equal to the number of bits that are removed from the CPS-PDU for the introduction of the new delineation field DF, that is, 8 bits from the STF field and 8 bits for each CPS packet in the CPS-PDU payload. Let N_{DF} be equal to the size, in bits, of the resulting delineation field DF. Then the overhead ratio, Γ, is defined as

$$\Gamma = \frac{N_{DF}}{N_r}. \tag{35}$$

It is clear that if $\Gamma > 1$ then the overhead introduced by the new delineation field is greater than the overhead removed, N_r.

Table 3: Sample set for vector sequence S_i.

α	Vector Sequence S_i
1	010000000000000000000000000000000000000000000000
2	010000000000000000000000010000000000000000000000
3	010000000000000001000000000000000100000000000000
4	010000000000010000000000010000000000010000000000
5	010000000010000000010000000010000000010000000000
6	010000000100000001000000010000000100000001000000
7	010000001000000100000010000001000000100000010000
8	010000010000010000010000010000010000010000010000
9	010000100001000010000100001000010000100001000000
10	010000100001000010000100001000010000100001000010
11	010001000100010001000100010001000100010001000000
12	010001000100010001000100010001000100010001000100

Table 3 shows a set of vector sequences S_i for the evaluation of the overhead ratio, Γ, as a function of the number of CPS-Packets, α, in the CPS-PDU payload. It should be noted that the set of sequences S_i shown in Table 3, is ideal for the evaluation of the overhead ratio Γ, as they include all possible worst-case scenarios for a given matrix **D**. In other words, by evaluating these sequences, it is possible to analyze all those cases in which a minimum amount of overhead N_r, is removed from the CPS-PDU while the size of the delineation field N_{DF} is maximized.

Table 4: Overhead ratio, Γ, for a given matrix D.

Matrix **D**	Number of CPS-Packets, α												
	0	1	2	3	4	5	6	7	8	9	10	11	12
24 × 2	4	2	1.33	1	0.8	0.67	0.71	0.63	0.56	0.5	0.45	0.42	0.38
16 × 3	3	1.5	1	1	0.8	0.67	0.57	0.63	0.56	0.5	0.45	0.5	0.46
12 × 4	2	1.5	1	0.75	0.6	0.67	0.57	0.5	0.44	0.5	0.45	0.42	0.38
8 × 6	2	1	1	0.75	0.8	0.67	0.71	0.63	0.67	0.5	0.55	0.42	0.46
6 × 8	1	1	1	0.75	0.8	0.83	0.71	0.63	0.56	0.5	0.45	0.42	0.38
4 × 12	1	1	1	1	1	0.83	0.71	0.63	0.56	0.5	0.45	0.42	0.38
3 × 16	1	1	1	1	0.8	0.67	0.57	0.5	0.44	0.4	0.36	0.33	0.31
2 × 24	1	1	1.33	1	0.8	0.67	0.57	0.5	0.44	0.4	0.36	0.33	0.31

From the list of possible vector sequences S_i, shown in Table 3, and assuming the largest Huffman codes for a given matrix **D**, shown in Table 2, it follows that it is possible to evaluate the overhead ratio Γ as a function of the number of CPS Packets α and the order of matrix **D**, as shown in Table 4. The selection of matrix **D** of order 24×2, 16×3, 12×4, 8×6 or 2×24 are not the best selections, as they have at least one case for which the overhead introduced by the delineation field is greater than the removed overhead N_r. From the remaining options, namely 6×8, 4×12 and 3×16, it is observed that matrix **D** of order 3×16 provides the best performance in terms of overhead reduction, as shown in Figure 47.

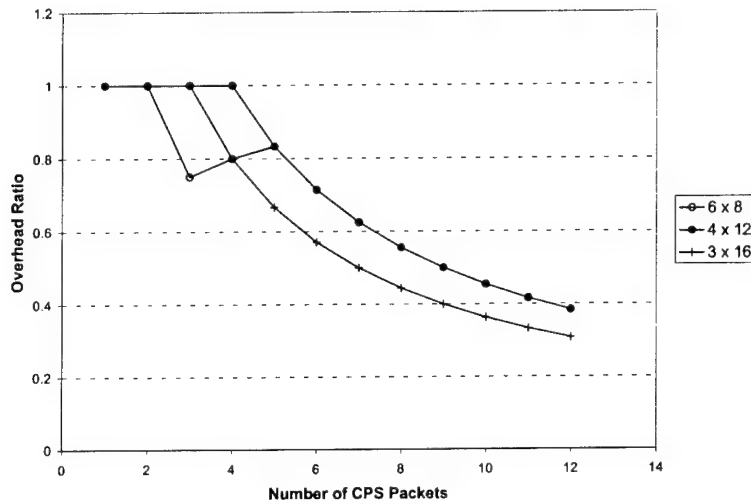*Figure 47: Overhead Ratio, Γ.*

For a matrix **D** of order 3×16, the overhead in bytes as a function of the number of CPS-Packets is shown in Figure 48.
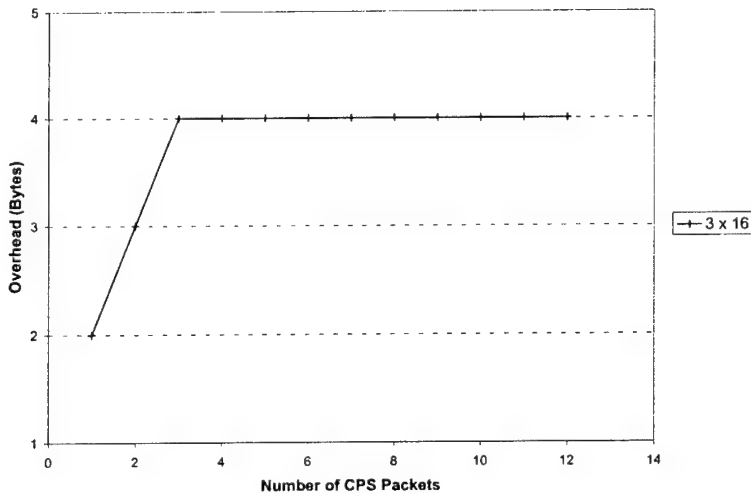

Figure 48: Delineation Field, DF, for Matrix D (3×16).

From Figure 48, it is observed that the size of the delineation sequence, *DS*, will range from 2 to 4 bytes depending on the number of CPS Packets. This requires a 2-bit delineation sequence length indicator (*DSLI*) to be included along with the *DS*. The proposed values for the length indicator and their description are presented in Table 5.

Table 5: Delineation sequence length indicator.

DSLI	DS field length, l_{DS}
0 0	$l_{DS} = 1$ byte
0 1	$l_{DS} = 2$ bytes
1 0	$l_{DS} = 3$ bytes
1 1	$l_{DS} = 4$ bytes

Figure 49, shows the structure of the Delineation Field, *DF*, in the CPS-PDU under the proposed delineation scheme. It should be noted that results presented in Table 4, Figure 47 and Figure 48 have accounted for the introduction of the *DSLI* field, as part of the *DF* field. Furthermore, a *DSLI* of size 3-bits is required for those cases in which matrix **D** has a dimension of 24×2, 16×3, 12×4 or 8×6, as it is not possible to represent all possible lengths for the resulting *DS* field with only 2-bits.

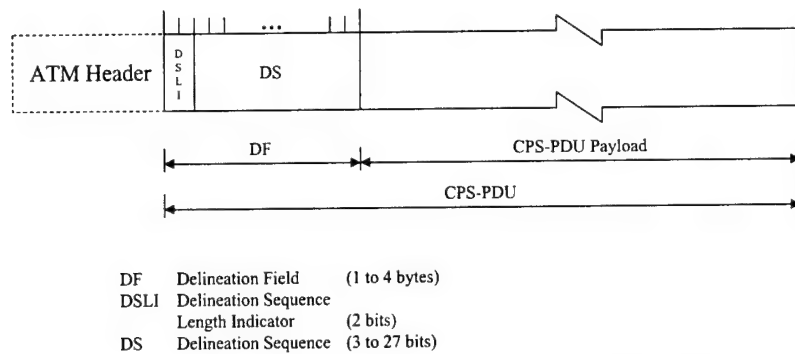|		
DF	Delineation Field	(1 to 4 bytes)
DSLI	Delineation Sequence Length Indicator	(2 bits)
DS	Delineation Sequence	(3 to 27 bits)

Figure 49: CPS-PDU format using the DF field.

The interoperability of the proposed scheme with standard AAL2 is not difficult to implement as both protocols provide the same functionality and they only differ on the mechanism used to achieve CPS-Packet delineation within the CPS-PDU.

7.4.4 Numerical Results over the Gilbert-Elliott Channel

Numerical results for performance measures *mCLR* and *mPER*, derived in Equations (28) and (30), are presented in this section. Results for performance metric *mPBER* are not presented due to the fact that results obtained for this performance metric are similar to those of metric *mCLR*. For consistency with results presented in Section 7.2, the following channel parameters were used for the Gilbert-Elliott model: steady state channel BER is $\varepsilon = 10^{-3}$ and state bit error probabilities are $P_e(0) = 0$ and $P_e(1) = 0.5$.

Figure 50(a) and Figure 50(b) show performance results for measure *mCLR* and *mPER* respectively, as a function of the mean burst length τ, for each of the CPS Packets in the CPS-PDU for the case CPS-PP of size 24 bits, $N = 7$, under the proposed delineation mechanism. For comparison purposes, Figure 50(c) and Figure 50(d) show the same performance results obtained under standard AAL2 CPS packet delineation.

Figure 50: Performance results for CPS-PP size 24 bits.

Figure 51(a) and Figure 51(b) show performance results for measure *mCLR* and *mPER* respectively, as a function of the mean burst length τ, for each of the CPS Packets in the CPS-PDU for the case CPS-PP of size 96 bits, $N = 3$, under the proposed delineation mechanism. For comparison purposes, Figure 51(c) and Figure 51(d) show the same performance results obtained under standard AAL2 CPS packet delineation.
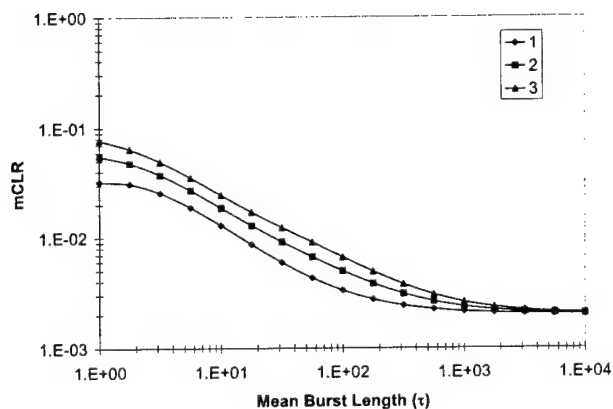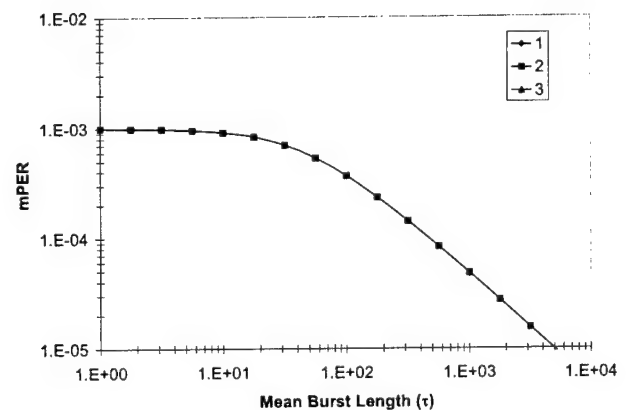
Figure 51: Performance results for CPS-PP size 96 bits.

Figure 52(a) and Figure 52(b) show average performance results for measure *mCLR* and *mPER* respectively, as a function of the mean burst length τ, for each of the CPS Packets in the CPS-PDU for the case CPS-PP of size 24, 96 and 352 bits, under the proposed delineation mechanism. For comparison purposes, Figure 52(c) and Figure 52(d) show the same performance results obtained under standard AAL2 CPS packet delineation.
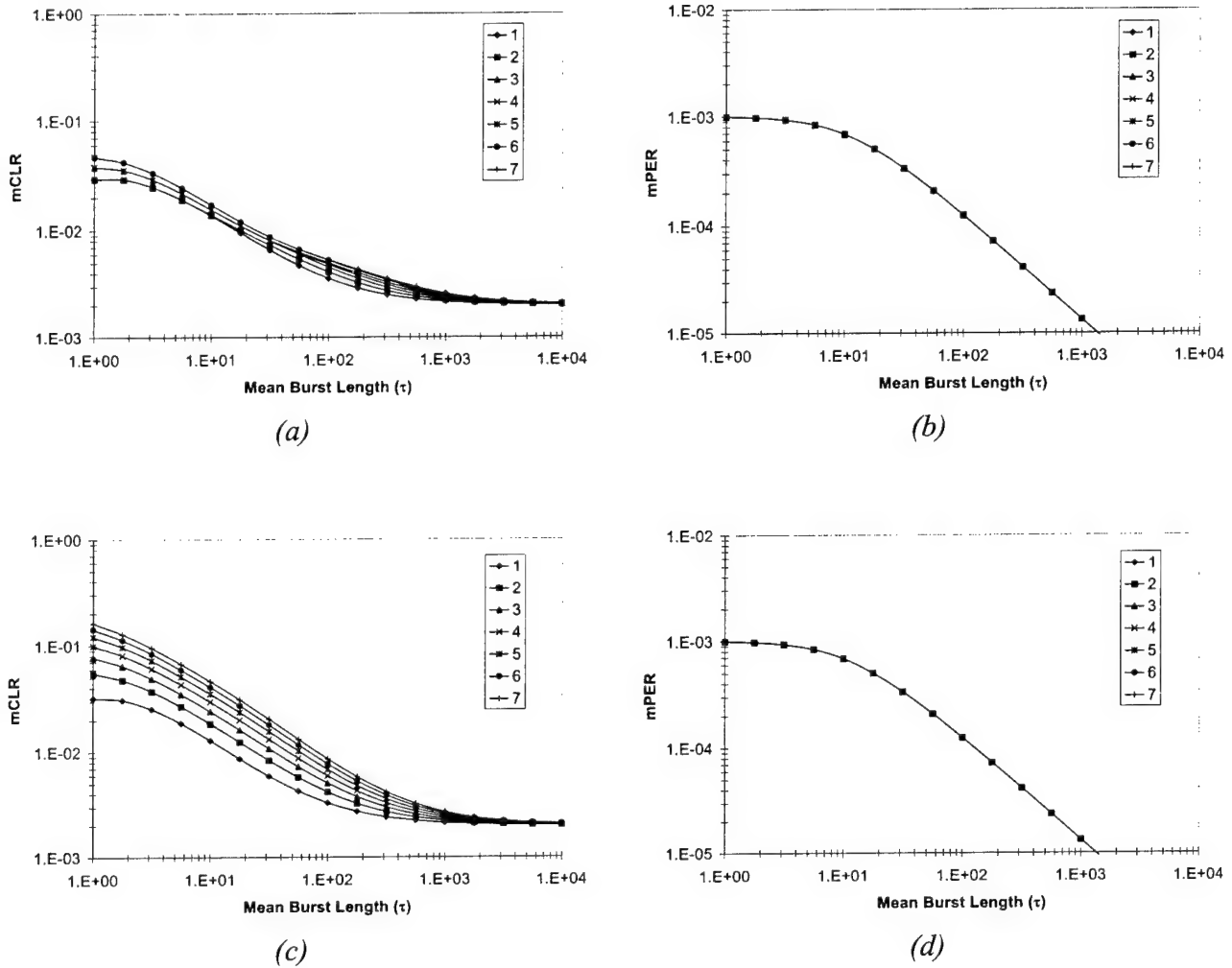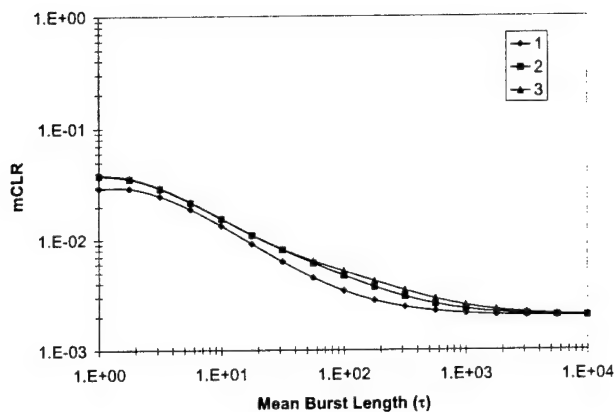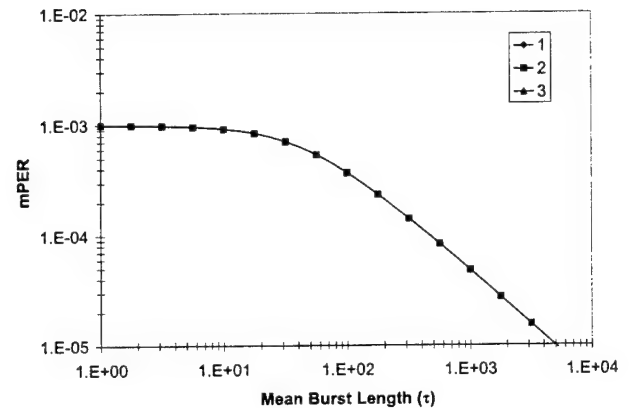

(a)

(b)
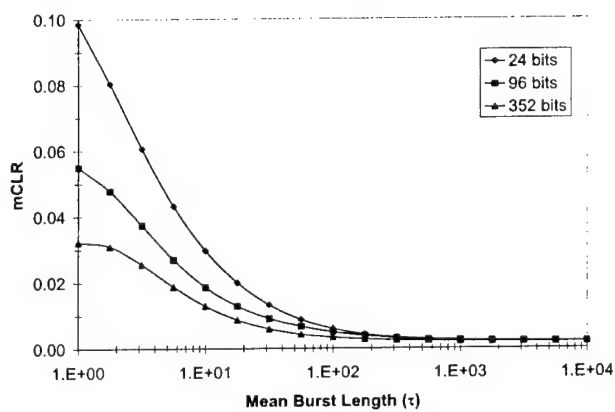
(c)

(d)

Figure 52: Average performance results.

By comparing the performance results obtained using the proposed delineation mechanism against the results obtained under standard AAL2 delineation, it is observed that 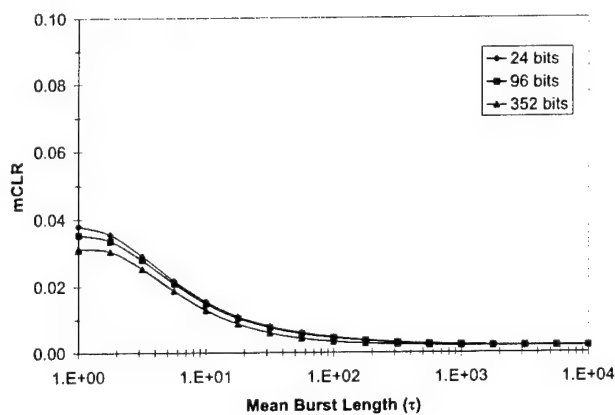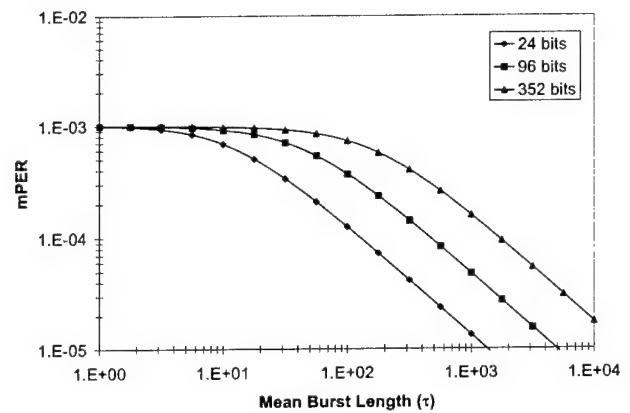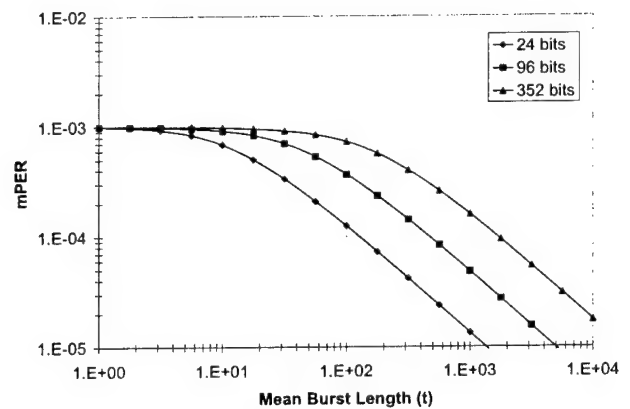under the proposed delineation mechanism the probability that a CPS packet will be lost, due to corrupted delineation fields, becomes more uniform (for a given mean burst length τ) for any CPS packet regardless of its relative position within the CPS-PDU or the size of the CPS packet payload. For example, in Figure 50(c) under standard AAL2 delineation, the probability that the first CPS packet will get lost, for a mean burst length $\tau = 1$, is equal to 0.03 (or 3%), while the probability that the last CPS packet is lost is 0.16 (or 16%). On the other hand, in Figure 50(a) under the proposed delineation mechanism, the probability that the first CPS packet will get lost, for a mean burst length $\tau = 1$, is equal to 0.03 (or 3%), while the probability that the last CPS packet is lost is less than 0.05 (or 5%).

Remarks:

- Numerical results presented in this section demonstrate that the proposed delineation mechanism improves the performance of AAL2 in the presence of bit errors. This gain in performance is achieved by "equalizing" the performance results of every AAL2 packet, regardless of their relative position within the payload of the CPS-PDU. Numerical results presented in sections 7.2 and 7.3 have shown that under metric $mCLR$ (probability of lost AAL2 packet) the first AAL2 packet immediately after the STF field has a better performance than the last CPS packet within the CPS-PDU payload. Under the proposed delineation mechanism this is no longer the case.

- The implementation of the proposed delineation mechanism reduces the overhead required by delineation header fields when the number of AAL2 packets within the CPS-PDU payload is greater than 3.

- The proposed delineation mechanism is compatible with standard AAL2, therefore allowing for interoperability over standard ATM networks.

7.5 Performance Results for AAL2 using Space Diversity

The analytical results presented in this section follow the implementation of a Finite State Markov Chain (FSMC) model using the Nakagami-m distribution for the characterization of the statistical time varying fading dynamics of the channel. One interesting characteristic of the Nakagami-m distribution is that it includes the *Rayleigh* distribution, as a special case ($m = 1$), and it also approximates the *Ricean* and *Lognormal* distributions [11]. Thus, analytical derivations following the Nakagami-m distribution can easily be generalized to evaluate the *Rayleigh* and the *Ricean* fading channels. The probability and joint density functions distributions of a Nakagami-m distributed random variable are given by

$$p_A(\alpha) = \frac{2\alpha^{2m-1}}{\Gamma(m)}\left(\frac{m}{\Omega}\right)^m \exp\left[-\frac{m\alpha^2}{\Omega}\right],$$ (36)

$$p_{A_1,A_2}(\alpha_1,\alpha_2) = \frac{4(\alpha_1\alpha_2)^m \exp\left[-\frac{m}{\Omega}\frac{\alpha_1^2+\alpha_2^2}{1-\rho}\right]}{\Gamma(m)(1-\rho)(\sqrt{\rho})^{m-1}}\left(\frac{m}{\Omega}\right)^{m+1} I_{m-1}\left\{\frac{2m\alpha_1\alpha_2\sqrt{\rho}}{\Omega(1-\rho)}\right\},$$ (37)

where $\Omega = \overline{\alpha^2}$ is the mean-square value of the fading amplitude α, m represents the Nakagami-m fading parameter, $\Gamma(\cdot)$ represents the Euler gamma function, $I_m\{\cdot\}$ represents the m-th order modified Bessel function of the first kind and ρ is the correlation coefficient between fading amplitudes α_1 and α_2.

The analysis assumes scattered waves arriving with a uniform angular distribution at the receiver node (*Rayleigh* fading). In this case the correlation coefficient, ρ, is defined as

$$\rho = J_0^2[2\pi f_d\tau],$$ (38)

where J_0 is the zero-order Bessel function of the first kind, f_d is the Doppler frequency and τ is equal to channel symbol duration.

Furthermore, the analysis assumes Equal Gain Combining (EGC) diversity for the improvement of system performance degradation at the receiver node. Under EGC diversity, if each of the L diversity branches is described by a Nakagami-m distributed random variable with parameters m_0 and Ω_0, then the combined output approximately follows a new Nakagami-m distribution [15] with parameters

$$m \cong Lm_0,$$ (39)

$$\Omega = L\Omega_0 + L(L-1)\Omega_0 \frac{\Gamma^2(m_0 + 1/2)}{m_0\Gamma^2(m_0)}, \qquad (40)$$

and the fading correlation parameter ρ, assuming the existence of i.i.d. (independent and identical distributed) diversity branch signals, of the diversity-combined output is equal to the correlation coefficient before equal gain combining [11], which is given by equation (38).

Numerical results for performance measures *mCLR*, *mPBER* and *mPER*, shown in Equations (28)-(30), demonstrate the performance of AAL2 over a correlated fading channel in the presence of Equal Gain Combining (EGC) diversity reception. The CPS-PDU structure shown in Figure 53 is considered for the derivation of numerical results ($M = 0$) and CPS Packets are assumed to be of equal size. The FSMC model is composed of a 6-state Markov chain and the average signal-to-noise (S/N) ratio was set to 23.8 dB for an average channel BER of 10^{-3}.
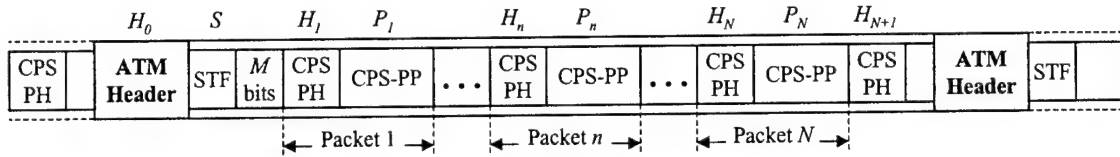
Figure 53: CPS PDU structure.

Performance results, presented in Figure 54 - Figure 56, show the case in which diversity is not used and assume a CPS-PDU composed of seven AAL2 packets, each with CPS PDU payload of size equal to 24 bits (3 bytes). Figure 54 shows results for metric *mCLR*, for CPS Packets 1 through 7, as a function of the argument $2\pi f_d\tau$, which is related to the behaviour of the fading process.
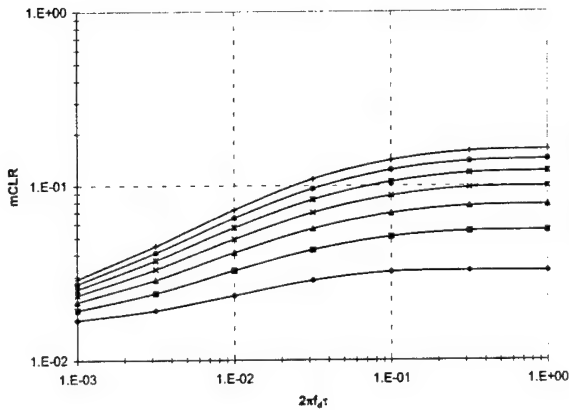
Figure 54: mCLR results for CPS Packets 1 through 7 (no diversity).
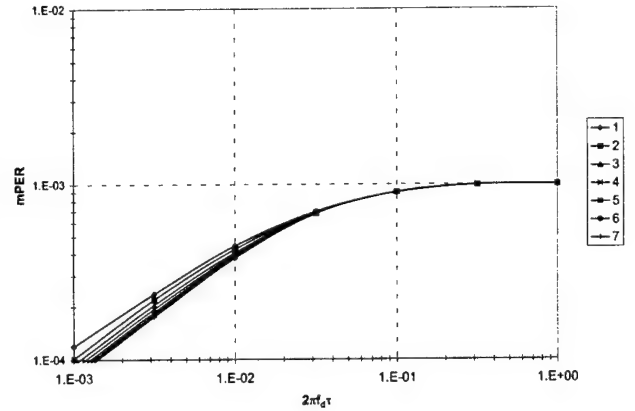
Figure 55: mPER results for CPS Packets 1 through 7 (no diversity).

From Figure 54 it is clear that the *mCLR* performance is best for CPS packet 1 and degrades with each subsequent CPS packet in the CPS-PDU payload. This behaviour is explained in view of the fact that the successful delivery of the CPS packet to the higher layers requires that the header of the

CPS packet be correct, and in addition, that all headers from previous CPS Packets in the CPS-PDU payload be correct.

Figure 56: mPBER results for CPS Packets 1 through 7 (no diversity).

Results for performance metric *mPER* are shown in Figure 55. From this figure it is observed that performance *mPER* degrades, as argument $2\pi f_d\tau$ increases (fast fading), until it converges to a value of *mPER* = 10^{-3}. Whereas for low values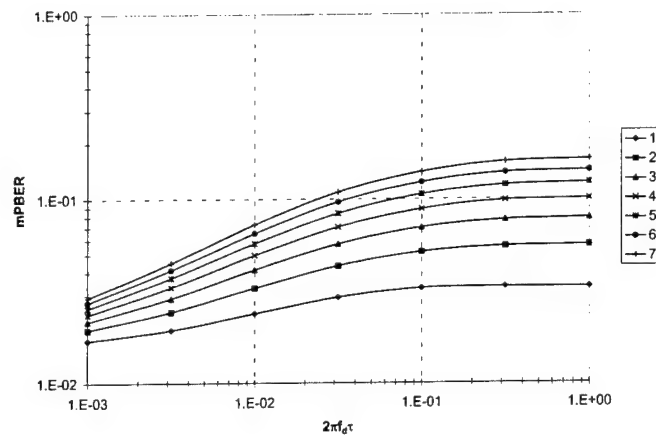 of argument $2\pi f_d\tau$ (slow fading), performance metric *mPER* improves for each CPS-Packet. This result is explained by the fact that under slow fading if the channel falls in a deep fade then the receiver will experience a long burst of errors. As the model BER is fixed this implies that long burst error periods are followed by equally long error-free periods thus reducing the probability of lost/discarded AAL2 Packets. On the other hand, under fast fading the channel tends to behave like a random channel as the receiver experiences short but frequent bursts of errors, therefore the probability of corrupted ATM/AAL2 headers increases. It is important to recall that a CPS packet can be mapped across CPS-PDU payload boundaries; in this case, the CPS packet is split in two parts, which are conveyed by two separate ATM cells. Performance measures for this scenario are not addressed in this study, but the results are expected to be worse than those in the case where a CPS packet is conveyed in a single ATM cell, as the successful delivery of the CPS packet requires the correctness of two rather than one ATM cell headers.

Figure 56 shows performance results for metric *mPBER*. It should be noted that performance results obtained for this metric are very similar to the results obtained for *mCLR*. From this observation it is clear that the main factor contributing to the BER seen by the higher layer is the *mCLR*, more specifically, the payload errors due to discarded CPS Packets. Recall that, by definition of *mPBER*, bits lost at the ATM/AAL2 are considered bit errors at the higher protocol layers.

Figure 57 and Figure 58 show performance results for metrics *mCLR* and *mPER* for the case with EGC diversity using two diversity branches (i.e. two antennas). Performance results for metric *mPBER* are not presented, as they are similar to the results obtained for metric *mCLR*. Numerical results show that the average BER, experienced by the ATM/AAL2 layers, has dropped to approximately 4.5×10^{-6}, which is more than two orders of magnitude compared to the case where diversity is not used. From Figure 57 it is observed that the probability of a lost AAL2 packet has dropped below 10^{-3}, whereas for the case with no diversity *mCLR* is greater than 10^{-2}, therefore the quality of voice transmission is improved, as voice communication is usually considered good for BER < 10^{-3}.
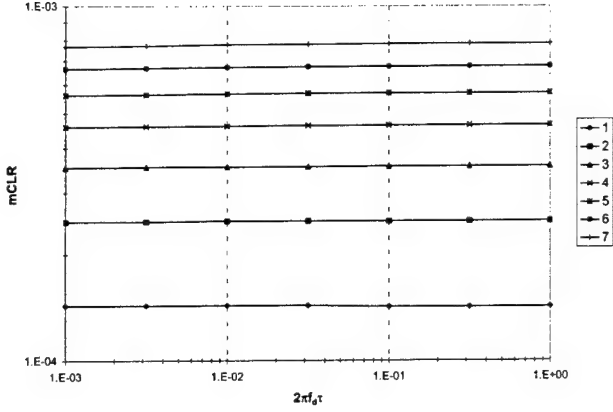
Figure 57: mCLR results for CPS Packets 1 through 7 (using 2 branch diversity).
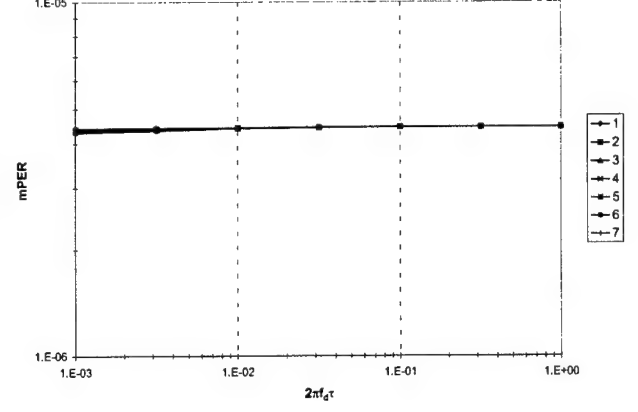
Figure 58: mPER results for CPS Packets 1 through 7 (using 2 branch diversity).

Since AAL2 can accommodate CPS Packets of variable payload size, it is of interest to study the performance of AAL2 over the wireless channel for CPS Packets with different payload sizes. For this purpose, numerical results for CPS Packets with payload size equal to 24, 96 and 352 bits are presented in Figure 59 and Figure 60. The results shown in these figures represent the average values over all CPS Packets that are carried in the CPS-PDU payload for the case with no diversity. The CPS-PDU payload carries 7, 3 or 1 complete CPS Packets for payloads of size 24, 96 or 352, respectively.

Figure 59: mCLR results for different CPS-PP size (no diversity).
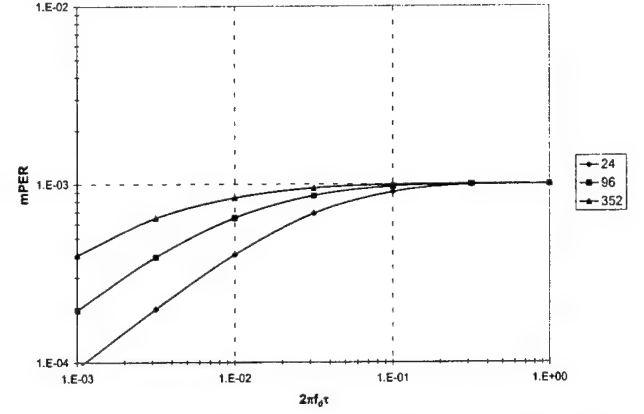
Figure 60: mPER results for different CPS-PP size (no diversity).

From Figure 59 it is observed that performance with respect to metric *mCLR* improves for large CPS Packets. For large CPS packet payloads, the number of CPS Packets that are carried in the CPS-PDU decreases and so does the number of CPS packet headers, thus the probability of corrupted headers affecting the CPS packet delineation decreases. In Figure 60, contrary to the behaviour exhibited by *mCLR*, the performance with respect to *mPER* improves for CPS Packets with small payload size. By definition, mPER is associated with the rate of errors in the CPS packet payload given that the header/control fields are correct, therefore it mainly depends on the impact of the error process over the CPS packet payload. Consequently, the probability of errors in the CPS packet

51

payload increases with the size of the payload field.

Performance results presented in Figure 61 and Figure 62 analyze the same performance metrics presented in Figure 59 and Figure 60 for the case in which EGC diversity with two diversity branches is implemented. In Figure 61 performance results for metric *mCLR* show that the probability of a lost CPS packet is below 10^{-3} regardless of the CPS packet payload size. Furthermore, it is observed that *mCLR* performance remains constant as argument $2\pi f_d\tau$ varies, thus the introduction of EGC diversity results in a mechanism resilient to fading variations. Figure 62 shows performance results for metric *mPER*, in this case it is observed that the probability of errors over the payload of a CPS packet remains the same regardless of the size of the CPS packet payload.
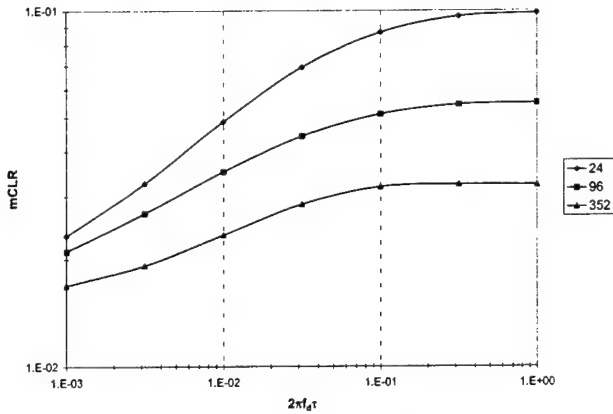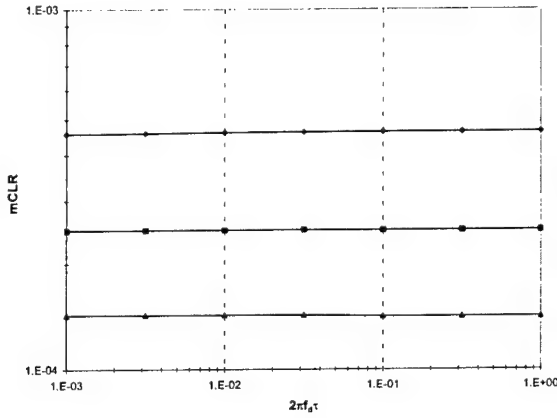

Figure 61: mCLR results for different CPS-PP size (2 branch diversity).
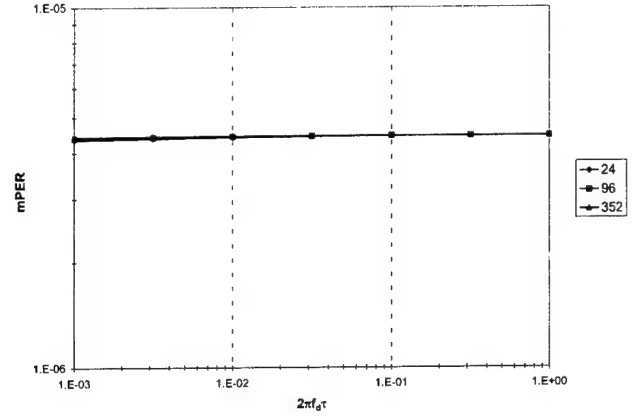
Figure 62: mPER results for different CPS-PP size (2 branch diversity).

Remarks:

- Numerical results have shown that the implementation of two branch Equal Gain Combining (space diversity) greatly improves the performance of AAL2 over correlated fading channels. The introduction of space diversity has the effect of reducing the BER experienced by the ATM and AAL2 layers, consequently the probability of lost AAL2 packets or bit errors over the payload of AAL2 packets is reduced.

- An interesting observation is that the numerical results obtained for metrics *mCLR*, *mPBER* and *mPER* over the FSMC which models the fading dynamics of the channel provide a close resemblance to the results presented over the Gilbert-Elliot channel. That is, results obtained for large values of $2\pi f_d\tau$ (fast fading) seem to resemble the results obtained for small mean burst lengths over the Gilbert-Elliott channel. In the same way, performance results obtained for small values of $2\pi f_d\tau$ (slow fading) seem to resemble the results obtained for large mean burst lengths over the Gilbert-Elliott channel.

52

8 AAL2 RECOMMENDATIONS

The main objective of this work is to present a study on the ATM Adaptation Layers for the transport of low data rate and delay sensitive traffic, such as voice, over tactical wireless ATM networks. In particular we present the study and performance evaluation of the ATM Adaptation Layer type 2, standardised by the ITU-T.

In this work several mechanisms, designed to reduce the *bit error rate* (BER) experienced by the layers above the AAL2, are analysed and numerical results are presented to demonstrate the impact of bit errors over such schemes. These mechanism include the use of: *Forward Error Correction* (FEC) codes to protect the ATM and AAL2 header fields, a new delineation mechanism for AAL2 and the use of space diversity techniques.

Based on the results presented in Section 7 the following observations and recommendations are made regarding the performance of AAL2:

- Under the standard ATM/AAL2 frame structure, the BER experienced by the layers above the AAL2 is mostly due to the impact of bit errors over ATM/AAL2 headers. That is, the main factor contributing to the performance degradation of AAL2 is the result of lost or discarded AAL2 packets due to non-correctable errors over ATM/AAL2 header fields. Furthermore, the delineation mechanism provided in standard AAL2 is vulnerable to bit errors. Numerical results show that the first AAL2 packet after the STF field achieves better performance (as indicated under measures *mCLR* and *mPBER*) compared to the last AAL2 packet in the CPS-PDU payload. These results suggest the need for implementation of some type of protection for ATM/AAL2 header fields and/or the implementation of a robust delineation mechanism to reduce the performance degradation of AAL2 due to the inherent dependency of AAL2 CPS packets.

- With respect to the use of *Forward Error Correcting* codes, numerical results demonstrate that the protection of ATM/AAL2 fields using BCH codes do not provide for better performance results compared to results obtained for the standard ATM/AAL2 frame structure. This observation is particularly true for those schemes in which the ATM header and the STF field were protected by BCH codes. A third approach, presented in this study, is the use of BCH codes to protect the AAL2 CPS-PH, in addition to BCH encoded ATM and STF fields. Under this scheme, performance results for measure *mCLR* begin to improve significantly for small mean burst lengths in the order of $\tau \approx 1$ bit. However, numerical results show that reducing the probability of lost AAL2 CPS packets (measure *mCLR*) helps to reduce the performance degradation (measure *mPBER*) experienced by the users of the AAL up to a certain limit, which is shown to be equivalent to the channel BER. This limit is related to the number of payload bits that are lost due to discarded AAL2 packets and the probability of errors over the payload of AAL2 packets. Beyond this limit, bit errors over the payload of non-discarded AAL2 packets is more significant compared to the number of payload bits that are lost due to discarded AAL2 packets. This observation is explained by the fact the AAL2 CPS packet payload does not provide any error correction capability. In this way, the use of BCH codes to protect ATM/AAL2 header fields is only useful to a certain extent.

- Numerical results obtained under standard AAL2 delineation show that one of the main factors contributing to performance degradation is the relative position of AAL2 CPS packets carried within the payload of ATM cells. This observation is explained by the fact that AAL2 introduces a scheme required for the delineation of AAL2 CPS packets, which is vulnerable to bit errors. As a result of lost delineation, AAL2 packets are discarded and payload information is lost. In this work we present a new mechanism for the delineation of AAL2 packets within the payload of ATM cells. Numerical results show that the proposed delineation mechanism can achieves a uniform performance, as presented under measure *mCLR*, for all AAL2 CPS packets regardless of their position within the CPS-PDU payload. In addition, numerical results show that it is possible to reduce the overhead required by the delineation fields to allow for larger AAL2 CPS packets.

- In this work we present numerical results to demonstrate the performance of ATM/AAL2 over correlated fading channels using space diversity. Numerical results show that this technique reduces the BER experienced by the ATM and AAL2 layers. However the use of space diversity does not address the performance issues due to the delineation mechanism used in standard AAL2. Therefore the use of space diversity, in conjunction with the proposed delineation mechanism is recommended.

ACRONYMS

AAL	ATM Adaptation Layer	ISDN	Integrated Services Digital Network
AAL-SDU	AAL Service Data Unit	ITU	International Telecommunications Union
ATM	Asynchronous Transfer Mode		
ATM-SDU	ATM Service Data Unit	IWF	Interworking Function
AWGN	Additive White Gaussian Noise	LI	Length Indicator
BCH	Bose – Chaudhuri-Hocquenghem codes	LOS	Line-of-Sight
		mCLR	mini-Cell Loss Rate
BER	Bit Error Rate	mPBER	mini-cell Payload Bit Error Rate
BS	Base Station	mPER	mini-cell Payload Error Rate
CAS	Channel Associated Signalling	MSC	Mobile Switching Centre
CBR	Constant Bit Rate	MT	Mobile Terminal
CCS	Common Channel Signalling	OSF	Offset Field
CID	Channel Identifier	PBX	Public Branch Exchange
CPS	Common Part Sublayer	PDU	Protocol Data Unit
CPS-INFO	CPS Information Data	PSTN	Public Switched Telephone Network
CPS-PDU	CPS Protocol Data Unit		
CPS-PH	CPS packet Header	PVC	Permanent Virtual Connection
CPS-PP	CPS packet Payload	QoS	Quality of Service
CPS-SDU	CPS Service Data Unit	RAN	Radio Access Network
CPS-UUI	CPS User-to-User Indication	RAP	Radio Access Point
CS	Convergence Sublayer	RNC	Radio Network Controller
DF	Delineation Field	RS	Reed – Solomon codes
DSLI	Delineation Sequence Length Indicator	SAP	Service Access Point
		SAR	Segmentation and Reassembly
EGC	Equal Gain Combining	SDU	Service Data Unit
FSMC	Finite State Markov Chain	SN	Sequence Number
HEC	Header Error Control	SNP	Sequence Number Protection
IMT-2000	International Mobile Telecommunications for the year 2000	SNR	Signal-to-Noise Ratio
		SPVC	Soft-Permanent Virtual Connection

SSCS	Service Specific Convergence Sublayer	UUI	User-to-User Indication
SSCS-PDU	SSCS Protocol Data Unit	VBR	Variable Bit Rate
STF	Start Field	VC	Virtual Circuit
SVC	Switched Virtual Connection	VCC	Virtual Channel Connection
TDM	Time Division Multiplexer	VCI	Virtual Channel Identifier
UMTS	Universal Mobile Telecommunications System	VPI	Virtual Path Identifier
		WATM	Wireless ATM
UNI	User-to-Network Interface	WLAN	Wireless Local Area Network

REFERENCES

[1] ITU-T Recommendation I.363.1, "B-ISDN ATM Adaptation Layer Specification: Type 1 AAL", April 1997

[2] ITU-T Recommendation I.363.2, "B-ISDN ATM Adaptation Layer Type 2 Specification", August 1996

[3] ATM Forum Technical Committee, " ATM Trunking using AAL2 for Narrowband Services", Final Ballot, January 1999

[4] Ericson, "Requirements for AAL2 signalling needed for handling switched AAL2 connections", ITU-T, Contribution D.605 – 1/11, May 1998

[5] General DataComm, "A Management Briefing on Adapting Voice for ATM Networks: A Comparison of AAL1 Versus AAL2", 1997

[6] General DataComm, "A Management Briefing on Adapting Voice for ATM Networks: An AAL2 Tutorial", 1997

[7] Nokia, "Signalling Requirements for setting up AAL2 switched virtual connection in AAL2 networks", ITU-T, Contribution D.608 – 1/11, May 1998

[8] A. M. Chen, R. R. Rao, "On Tractable Wireless Channel Models", Proc. 9th IEEE International Symposium on Personal, Indoor and Mobile Radio Communications, Vol. 2, Sept. 1998, pp. 825-830

[9] E. N. Gilbert, "Capacity of a burst-noise channel", Bell Systems Technical Journal, Vol. 39, Sept. 1960, pp. 1253-1266

[10] E. O. Elliott, "Estimates of error rates for codes on burst-error channels", Bell Systems Technical Journal, Vol. 42, Sept. 1963, pp. 1977-1997

[11] Y. L. Guan, L. F. Turner, "Generalised FSMC model for radio channels with correlated fading", IEE Proceedings Communications, Vol. 146, No. 2, Apr. 1999, pp. 133-137

[12] H. S. Wang, N. Moayeri, "Finite-State Markov Channel – A Useful Model for Radio Communication Channels", IEEE Transactions on Vehicular Technology, Vol. 44, No. 1, Feb. 1995, pp. 163-171

[13] J. Lu, K. B. Letaief, M. L. Liou, "Robust Video Transmission over Correlated Fading Channels", IEEE Transactions on Circuits and Systems for Video Technology, Vol. 9, No. 5, Aug. 1999, pp 737-751

[14] M. K. Simon, M. Alouini, "Digital Communication over Fading Channels: A Unified Approach to Performance Analysis", Wiley-Interscience, 2000

[15]   M. Nakagami, "The m-Distribution – A General Formula of Intensity Distribution of Rapid Fading", Statistical Methods in Radio Wave Propagation, Jun. 1958, pp. 3-36

[16]   S. A. Abbas, A. U. Sheikh, "A Geometric Theory of Nakagami Fading Multipath Mobile Radio Channel with Physical Interpretations", IEEE 46th Vehicular Technology Conference, Apr. 1996, pp. 637-641

[17]   M. Zorzi, R. R. Rao, "On the Impact of Burst Errors on Wireless ATM", IEEE Personal Communications, Vol. 6, No. 4, Aug. 1999, pp. 65-75

[18]   M. Zorzi, R. R. Rao, "On the Statistics of Block Errors in Bursty Channels", IEEE Transactions on Communications, Vol. 45, No. 6, June 1997, pp. 660-667

DOCUMENT CONTROL DATA
(Security classification of title, body of abstract and indexing annotation must be entered when the overall document is classified)

1. ORIGINATOR (the name and address of the organization preparing the document. Organizations for whom the document was prepared, e.g. Establishment sponsoring a contractor's report, or tasking agency, are entered in section 8.) COMMUNICATIONS RESEARCH CENTRE CANADA 3701 CARLING AVENUE, PO BOX 11490, STATION H OTTAWA, ON K2H 8S2	2. SECURITY CLASSIFICATION (overall security classification of the document, including special warning terms if applicable) UNCLASSIFIED

3. TITLE (the complete document title as indicated on the title page. Its classification should be indicated by the appropriate abbreviation (S,C or U) in parentheses after the title.)

MILITARY VOICE SERVICES OVER WIRELESS ATM NETWORKS: ATM ADAPTATION LAYER STUDY (U)

4. AUTHORS (Last name, first name, middle initial)

VILLASENOR-GONZALEZ, LUIS; LAMONT, LOUISE

5. DATE OF PUBLICATION (month and year of publication of document) MARCH, 2001	6a. NO. OF PAGES (total containing information. Include Annexes, Appendices, etc.) xiv + 58	6b. NO. OF REFS (total cited in document) 18

7. DESCRIPTIVE NOTES (the category of the document, e.g. technical report, technical note or memorandum. If appropriate, enter the type of report, e.g. interim, progress, summary, annual or final. Give the inclusive dates when a specific reporting period is covered.)

TECHNICAL REPORT

8. SPONSORING ACTIVITY (the name of the department project office or laboratory sponsoring the research and development. Include the address.)

DEFENCE RESEARCH ESTABLISHMENT OTTAWA (DREO)
NATIONAL DEFENCE HEADQUARTERS, OTTAWA, ONTARIO, CANADA
K2H 8S2

9a. PROJECT OR GRANT NO. (if appropriate, the applicable research and development project or grant number under which the document was written. Please specify whether project or grant) 5cb17	9b. CONTRACT NO. (if appropriate, the applicable number under which the document was written)

10a. ORIGINATOR'S DOCUMENT NUMBER (the official document number by which the document is identified by the originating activity. This number must be unique to this document.) CRC-RP-2001-02	10b. OTHER DOCUMENT NOS. (Any other numbers which may be assigned this document either by the originator or by the sponsor) DREO-TR-2001-059

11. DOCUMENT AVAILABILITY (any limitations on further dissemination of the document, other than those imposed by security classification)

(X) Unlimited distribution
( ) Distribution limited to defence departments and defence contractors; further distribution only as approved
( ) Distribution limited to defence departments and Canadian defence contractors; further distribution only as approved
( ) Distribution limited to government departments and agencies; further distribution only as approved
( ) Distribution limited to defence departments; further distribution only as approved
( ) Other (please specify):

12. DOCUMENT ANNOUNCEMENT (any limitation to the bibliographic announcement of this document. This will normally correspond to the Document Availability (11). However, where further distribution (beyond the audience specified in 11) is possible, a wider announcement audience may be selected.)

UNLIMITED

13. ABSTRACT (a brief and factual summary of the document. It may also appear elsewhere in the body of the document itself. It is highly desirable that the abstract of classified documents be unclassified. Each paragraph of the abstract shall begin with an indication of the security classification of the information in the paragraph (unless the document itself is unclassified) represented as (S), (C), or (U). It is not necessary to include here abstracts in both official languages unless the text is bilingual).

(U) ATM technology has enjoyed great success, due in great part, for its ability to support a whole range of applications with Quality of Service (QoS) guarantees. Consequently, ATM has become of great interest for the support of services over military telecommunications networks.

(U) This report is provided as part of a study on the feasibility of military voice services over wireless ATM networks. In this study we are concerned with the support of low data rate and delay sensitive applications over wireless ATM link, where the ATM Adaptation Layer 2 has been identified as a suitable adaptation layer for the support of such type of traffic. Nevertheless, as currently specified, AAL2 does not provide any protection mechanisms to allow for its efficient implementation over the wireless medium. The work presented in this document includes performance analysis results to evaluate the implementation of Forward Error Correction (FEC) codes, diversity reception mechanisms and/or protocol enhancements to improve the performance of AAL2 over a wireless ATM network.

14. KEYWORDS, DESCRIPTORS or IDENTIFIERS (technically meaningful terms or short phrases that characterize a document and could be helpful in cataloguing the document. They should be selected so that no security classification is required. Identifiers such as equipment model designation, trade name, military project code name, geographic location may also be included. If possible keywords should be selected from a published thesaurus. e.g. Thesaurus of Engineering and Scientific Terms (TEST) and that thesaurus-identified. If it is not possible to select indexing terms which are Unclassified, the classification of each should be indicated as with the title.)

WIRELESS ATM
ATM ADAPTATION LAYER
VOICE OVER WIRELESS ATM
WIRELESS COMMUNICATIONS

Defence R&D Canada

is the national authority for providing
Science and Technology (S&T) leadership
in the advancement and maintenance
of Canada's defence capabilities.

R et D pour la défense Canada

est responsable, au niveau national, pour
les sciences et la technologie (S et T)
au service de l'avancement et du maintien des
capacités de défense du Canada.

DEFENCE **R·D** DÉFENSE

www.drdc-rddc.dnd.ca